Journal of Nanobiotechnology

RESEARCH

Open Access

# *Lactobacillus plantarum*-derived extracellular vesicles from dietary barley leaf supplementation attenuate *Citrobacter rodentium* infection and intestinal inflammation

Yu Feng[1], Qian Zhao[1], Yifan Zhao[1], Chen Ma[1], Meiling Tian[1], Xiaosong Hu[1], Fang Chen[1] and Daotong Li[1,2*]

## Abstract

**Background** Inflammatory bowel disease (IBD) is a gastrointestinal inflammatory disorder characterized by disturbed interactions between gut microbiota and host immune response. Barley leaf (BL) is a traditional Chinese herb recorded to have health-promoting effects. However, little is known about the beneficial role of BL against enteric infection-induced intestinal inflammation. Here, we uncover that BL protects against *Citrobacter rodentium* (*C. rodentium*)-induced infectious colitis by improving host-microbiota interactions.

**Methods** C3H/HeN mice were fed a diet with/without BL and infected with C. rodentium. Transcriptome sequencing, anti-CD4 antibody treatment, and flow cytometry were conducted to investigate the mechanisms of T cell immune modulation. The intervention involved administering anti-CD4 antibody at 500 μg each time for three times before and during *C. rodentium* infection. Analysis of gut microbiota composition was performed by 16S rRNA gene sequencing on fecal samples. Fecal microbiota transplantation was conducted by administering microbiota from donor group to recipient group via oral gavage to investigate the role of intestinal microbiota in immune modulation.

**Results** BL ameliorated the severity of *C. rodentium*-induced colitis, and this effect was linked to improved gut homeostasis and enhanced mucosal barrier function. BL enriched the pathways of T helper 1 (Th1)/Th2 and Th17 cell differentiation in the colon, suggesting the involvement of $CD4^+$ T cells. Consistent with this, anti-CD4 antibody treatment abrogated the effect of BL and flow cytometry analysis revealed that BL mitigated *C. rodentium*-induced pro-inflammatory Th1 immune response. Moreover, the protective effect of BL was associated with alleviation of gut microbiota dysbiosis and increased abundance of *Lactobacillus*. Our in vivo studies further revealed that live *Lactobacillus plantarum (L. plantarum)* administration attenuated the pathogenic effects induced by *C. rodentium* infection, whereas heat-inactivated *L. plantarum* did not show the same results. Mechanistically, BL supplementation

*Correspondence:
Daotong Li
lidaotong@cau.edu.cn

Full list of author information is available at the end of the article

enriched *L. plantarum*, which subsequently released nanosized extracellular vesicles (EVs) that serve as a key mediator in alleviating *C. rodentium*-associated pathology and Th1 cell dysregulation.

**Conclusions** Our work thus provides evidence for utilizing BL and *L. plantarum*-derived EVs to manage enteric infection-associated IBD.

**Keywords** Barley leaf, *Citrobacter rodentium*, Colitis, Th1 immune response, Extracellular vesicles

## Introduction

Inflammatory bowel disease (IBD) is a non-specific chronic recurrent inflammatory disease characterized by abdominal pain and diarrhea, bloody stool, and weight loss [1, 2]. Epidemiological evidence has shown that the prevalence and incidence of IBD are raising every year, especially in newly industrialized countries; and thus becomes a public threat and burden to human health [3–5]. The currently drug-based therapies in treating IBD showed limited effectiveness and potential side effects [6]. Therefore, there is an urgent need to develop novel and effective strategies for the management of IBD.

Though the etiology of IBD is still unclear, dysbiosis of gut microbiota have been implicated in the onset and progression of IBD [7–9]. The composition and function of gut microbiota could be shaped by diet, which is an important environmental factor associated with the epidemiology and pathogenesis of IBD [10, 11]. A recent study has shown that diet-based therapy is effective in improving gut microbiota dysbiosis and alleviating clinical outcomes in patients with ulcerative colitis [12]. Thus, dietary intervention may be a promising strategy that can be used in the prevention and treatment of IBD [13].

A wide range of pathogenic microbes are capable of entering the gastrointestinal tract, causing enteric infection and intestinal inflammation. Applying bacterial infection model is important to understand the fundamental role of dietary factors in host-microbe interactions [14–20]. *Citrobacter rodentium* (*C. rodentium*)-induced bacterial colitis has long been utilized as a robust model to study the role of commensal bacteria in pathogen-host interactions. *C. rodentium* infection triggers microbiota dysbiosis that is characterized by a reduced bacteria diversity and an over-expansion of *C. rodentium* by day 7 following infection [21]. *C. rodentium* colonization can be resisted by the commensal gut microbiota and the colonization resistance of the gut microbiota to *C. rodentium* is reliant on nutrient availability [22, 23]. For instance, deprivation of dietary fiber has been reported to promote susceptibility to *C. rodentium* via diet-driven changes in the gut microbiota [24]. Thus, dietary nutrients may serve as crucial factors to protect against *C. rodentium*-induced enteric infection.

Barley leaf (BL), the young leaf of *Hordeum vulgare L.*, is a traditional Chinese herb with historically documented potential health benefits. Dietary fiber, protein, polyphenols, vitamins, and minerals are the major ingredients of BL [25]. The antioxidative, antidepressant, and lipid-lowering properties have been reported [26, 27]. Our previous studies have demonstrated that dietary BL modulates gut microbiota, and protects against chemically-induced colitis and colon tumorigenesis [28–30]. However, the beneficial effect of BL on intestinal microbial communities in the context of bacterial colitis is unclear. Whether and how gut microbiota modulates the potential effects of BL on host susceptibility to enteropathogenic infection and intestinal inflammation remains elusive.

In this study, we applied murine pathogen *C. rodentium* to mimic a similar pathogenesis to human enterohemorrhagic and enteropathogenic *E. coli.* The beneficial effect of BL against *C. rodentium* infection and intestinal inflammation was investigated. Our results provided evidence to show that BL alleviated *C. rodentium*-induced colonic inflammation, barrier damage, and gut microbiota dysbiosis. Additionally, BL-induced protection was found to be dependent on $CD4^+$ T cells. We further revealed a crucial role of BL-induced gut microbiome in the modulation of protection against *C. rodentium* infection. Colonization of mice with live but not heat-inactivated *Lactobacillus plantarum (L. plantarum)*, a commensal bacterium greatly enriched by BL, was sufficient to recapitulate the protection against *C. rodentium* infection. Mechanistically, *L. plantarum*-released extracellular vesicles (EVs) alleviated *C. rodentium*-induced bacterial colitis and T cell dysregulation in mice. This study provided novel insights into the potential immunoregulatory properties of BL and probiotic-derived EVs for developing effective therapeutic treatment in enteric infection and inflammation.

## Results

### BL attenuates intestinal pathology in *C. rodentium*-infected mice

To evaluate whether BL conferred protective effects against *C. rodentium*-induced colonic inflammation, mice were fed with a standard chow diet or an isocaloric diet supplemented with BL for 3 weeks and inoculated or not with *C. rodentium* (Fig. 1A). Food consumption and water intake were monitored daily prior and during the infection. Our results showed that there was no significant difference in food intake or water intake between

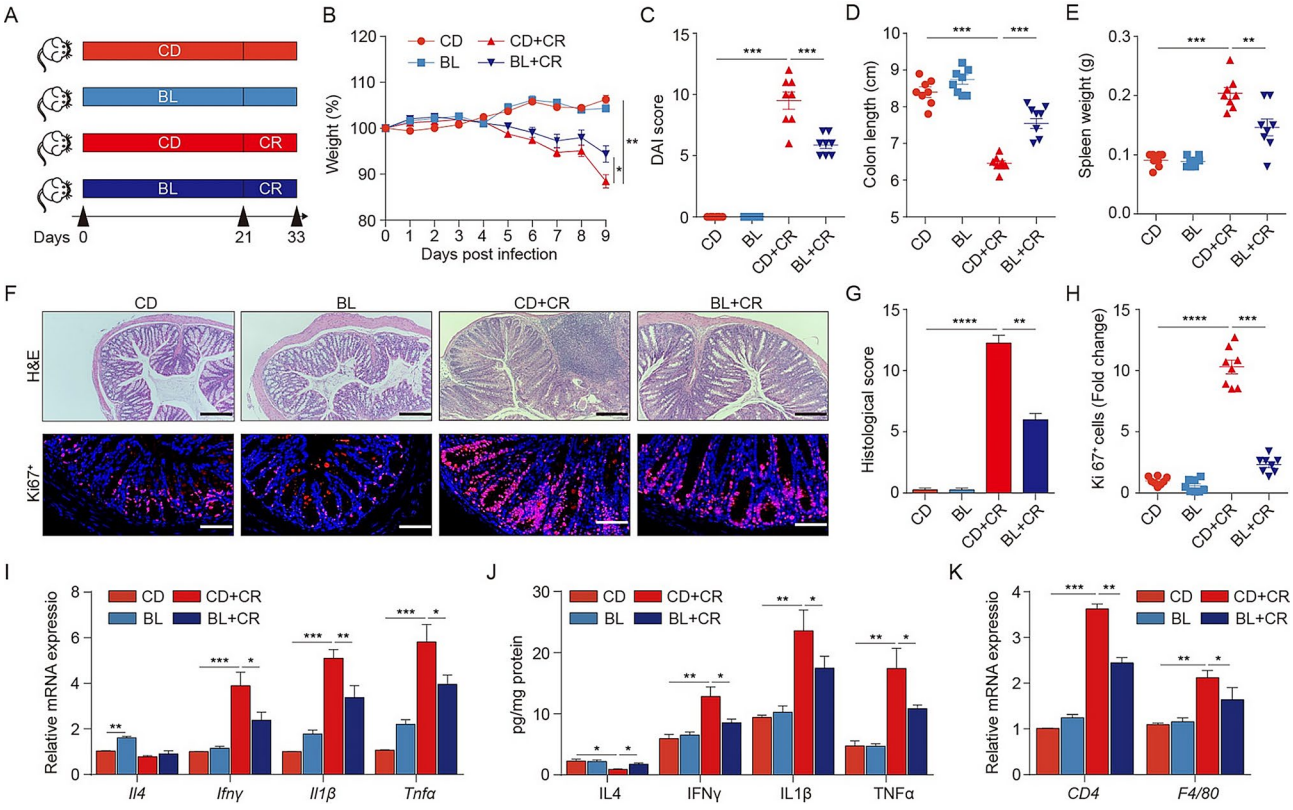


**Fig. 1** Barley leaf (BL) attenuates *C. rodentium* (CR)-induced colitis. (**A**) Study design of in vivo mouse experiment. Mice were fed with a standard chow diet (CD) or an isocaloric BL-supplemented diet for 3 weeks prior to the infection with CR for 10 days. (**B**) Body weight change. (**C**) Disease activity index (DAI) scores. (**D**) Colon length. (**E**) Spleen weight. (**F**) Representative hematoxylin and eosin (H&E) staining images of colon tissues. Scale bar, 100 μm. Representative Ki67-stained immunofluorescence images of colon tissues. Scale bar, 50 μm. (**G**) Histological scores. (**H**) Quantification of Ki67 positive cells. (**I**) The mRNA expression of *Ifnγ*, *Il1β*, and *Tnfa* in the colon. (**J**) The levels of IFN-γ, IL-1β, and TNF-α in the colon. (**K**) The mRNA expression of CD4 and F4/80 in the colon. In (**B**) - (**H**), ($n = 8$ per group). In (**I**) - (**K**), ($n = 6$ per group). Data are mean ± SEM. $^{*}P < 0.05$, $^{**}P < 0.01$, $^{***}P < 0.001$ and $^{****}P < 0.0001$. For body weight change, a repeated measure two-way analysis of variance (ANOVA) was performed and the rest of the statistics were performed with one-way ANOVA followed by Tukey's multiple comparison's test

BL- and chow diet (CD)-fed mice, suggesting that BL supplementation had no adverse effect on the mouse eating and drinking habits (Figure S1). Compared to control uninfected mice, mice infected with *C. rodentium* exhibited significant body weight loss and increased disease activity index (DAI) score (Fig. 1B and C). The colon length was shorter and the spleen weight was greater in *C. rodentium*-infected mice compared to control uninfected mice (Fig. 1D and E; Figure S2). Nevertheless, the above deleterious effects caused by *C. rodentium* were attenuated in BL-fed mice (Fig. 1B-E). Histological analysis of colonic sections showed that *C. rodentium* infection led to pathologic changes, such as colonic thickening, epithelial injury, and inflammatory cell infiltration; these histologic damages were remarkably attenuated in BL-fed mice (Fig. 1F and G; Figure S2). We next analyzed the effect of BL on colonic hyperplasia, a hallmark of *C. rodentium* infection [15]. The number of colonic Ki67$^{+}$ cells was dramatically reduced in *C. rodentium*-infected mice fed with BL (Fig. 1F and H).

In addition to assessing pathological alterations in the colonic epithelium, the effect of BL on inflammatory factors was also examined. Compared to control uninfected mice, *C. rodentium*-infected mice showed significantly increased expression of *Ifnγ*, *Il1β*, and *Tnfα* in the colon at day 10 after infection; while BL downregulated these inflammatory cytokines but had no effect on the mRNA level of *IL-4* (Fig. 1I). Correspondingly, the elevated levels of IFN-γ, IL-1β, and TNF-α caused by *C. rodentium* infection were mitigated in BL-fed mice (Fig. 1J). Moreover, BL reduced the upregulated expression of CD4$^{+}$ T cell marker CD4 and macrophage marker F4/80 in the colon of *C. rodentium*-infected mice, suggesting that BL suppresses *C. rodentium*-induced inflammatory responses (Fig. 1K). Collectively, these findings suggest that BL alleviates colonic injury and improves intestinal inflammation in *C. rodentium*-infected mice.

### BL attenuates pathogen colonization and improves gut barrier function

After the oral gavage, *C. rodentium* initially colonizes the cecum and then migrates to the colon [17]. The severity of intestinal pathology during infection is primarily driven by colonization and virulence potential. To investigate whether BL attenuated *C. rodentium* colonization during infection, we measured the pathogen burden in *C. rodentium*-infected mice. BL supplementation significantly reduced the fecal *C. rodentium* loads on days 1, 4, 7, and 10 post-infection (Fig. 2A). Consistently, the bacterial counts in cecum content were significantly reduced in mice fed with BL on day 10 post-infection (Fig. 2B). Notably, the bacterial levels of *C. rodentium* in spleen and liver were also significantly lower in BL-fed mice than that in mice fed the control diet (Fig. 2C and D), suggesting that the systemic dissemination of enteric pathogen is mitigated by BL.

We speculated that BL might improve intestinal barrier function to inhibit the systemic translocation of *C. rodentium*. To test this hypothesis, we used real-time PCR to detect the expression of genes encoding tight junction proteins. We found that the mRNA expression of *Claudin1*, *Claudin2* and *ZO-1* was lower in *C. rodentium*-infected mice compared to control uninfected mice; while the expression of these genes was significantly elevated in mice fed with BL (Fig. 2E). Alcian blue staining revealed a reduction of mucus-producing goblet cells in the colon of *C. rodentium*-infected mice compared to that in control uninfected mice; whereas BL markedly ameliorated the loss of goblet cells caused by *C. rodentium* ($P < 0.05$) (Fig. 2F and G).

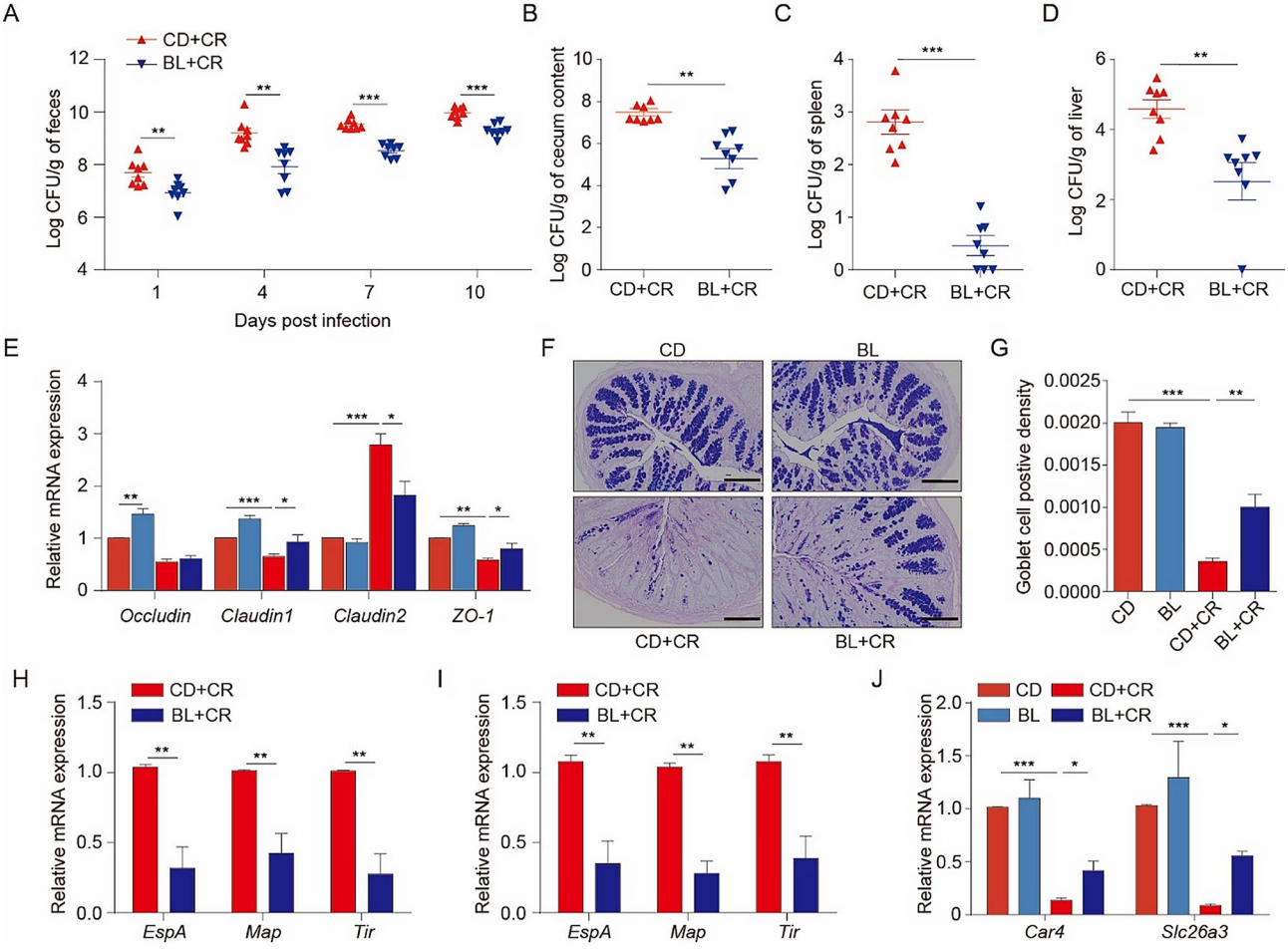


**Fig. 2** Barley leaf (BL) reduces the bacterial burden and improves the gut barrier function in *C. rodentium* (CR)-infected mice. (**A**) Number of CR in feces on days 1, 4, 7, and 10 post-infection. (**B**) Number of CR in cecum content on day 10 post-infection. (**C**) Number of CR in the spleen on day 10 post-infection. (**D**) Number of CR in liver on day 10 post-infection. (**E**) Real-time polymerase chain reaction (PCR) assay for the expression of *Occludin*, *Claudin1*, *Claudin2*, and *ZO-1* in the colon. (**F**) Representative images of alcian blue-stained colonic sections. Scale bar, 100 μm. (**G**) Quantification of mucusproducing goblet cells. (**H**) Real-time PCR assay for the expression of *EspA*, *Map*, and *Tir* in the colon. (**I**) Real-time PCR assay for the expression of *EspA*, *Map*, and *Tir* in the cecum. (**J**) Real-time PCR assay for the expression of *Car4* and *Slc26a3* in the colon. ($n = 8$ per group). Data are mean ± SEM. *$P < 0.05$, **$P < 0.01$ and ***$P < 0.001$. For (**E**), (**G**), and (**J**), statistical analysis was performed using one-way analysis of variance (ANOVA) followed by Tukey's multiple comparison's test, and the rest of the statistics were performed with Student's *t*-test

The transcriptional activation of Lee pathogenicity island encoding T3SS is required for the colonization of *C. rodentium* [16]. The LEE-encoded T3SS enables pathogens to inject their effectors into colonocytes [16]. We further examined the impact of BL on Lee-encoded virulence factors. As expected, the expression of *EspA*, *Map*, and *Tir* was increased in colon and cecum of *C. rodentium*-infected mice (Fig. 2H and I). However, these effects were significantly attenuated in BL-fed mice (Fig. 2H and I). In addition, BL supplementation significantly abrogated the reduced colonic expression of chloride anion exchanger *Sla26a3* and electrolyte absorption protein *Car4* in *C. rodentium*-infected mice (Fig. 2J). These results indicate that BL improves gut barrier function to prevent *C. rodentium* colonization and attenuates infection.

#### BL modulates T cell immune response pathway

To further dissect the mechanisms underlying the beneficial effect of BL, we performed a genome-wide transcriptome sequencing analysis on mouse colonic tissues. There were significant differences in mRNA gene expression profiles among the groups as revealed by PCA analysis and heat map of differentially expressed genes (DEGs) (Fig. 3A; Figure S3). Venn analysis showed that there were 2063 DEGs overlapped between CD group vs. CD + *C. rodentium* group and CD + *C. rodentium* group vs. BL + *C. rodentium* group (Fig. 3B). Volcano plot revealed that a total of 3841 (1815 upregulated genes and 2026 downregulated genes) and 3001 (1647 upregulated genes and 1354 downregulated genes) genes differed significantly in CD versus CD + *C. rodentium* group and in CD + *C. rodentium* versus BL + *C. rodentium* group ($P$ value < 0.05 and Fold change > 2), respectively (Fig. 3C). Notably, Th1/Th2 cell differentiation and Th17 cell differentiation were identified as the top significantly enriched KEGG pathways (Fig. 3D). Heat map analysis of DEGs on these pathways showed that *C. rodentium* treatment resulted in an increased expression of *Jag2*, *Rela*, *Cd247*, *Cd4*, *Lck*, *Cd3e*, *Jak3*, *Cd3d*, *Lat*, *H2-Ea*, *H2-Aa*, *H2-Ab1*, *H2-Eb1*, *H2-DMb2*, *H2-DMa*, *H2-DMb1* and *Ifng*, and a decreased expression of *Gata3*, *Mapk12* and *Mapk10*, and this was effectively reversed by BL (Fig. 3E). The interaction network of key genes in pathways of Th1/Th2 and Th17 cell differentiation was depicted by STRING analysis (Fig. 3F). Furthermore, real-time PCR was used to verify the expression of DEGs and the results were consistent with the transcriptome sequencing data (Fig. 3G). These data suggest that T cell immune response may contribute to the attenuated colitis in *C. rodentium*-infected mice fed with BL.

#### BL attenuates *C. rodentium* infection in a $CD4^+$ T cell-dependent manner

Previous studies have shown that adaptive T cell immune response is essential for defending against pathogen infection [19, 20]. However, it is unclear whether $CD4^+$ T cells were involved in protective effect of BL against *C. rodentium* infection. To test the involvement of $CD4^+$ T cells in beneficial effect of BL, the anti-CD4 antibody was administered prior and during *C. rodentium* infection (Fig. 4A). Consistent with previous results, mice fed with BL protected against *C. rodentium*-induced body weight loss, increased DAI scores, colon shortening, and splenomegaly; notably, this was not seen in BL-fed mice treated with anti-CD4 antibody (Fig. 4B-E). Furthermore, *C. rodentium*-induced colonic epithelial damage and mucosal barrier dysfunction were alleviated in mice fed with BL; while this was not observed when mice were treated with anti-CD4 antibody (Fig. 4F-H). The relieving levels of IFN-γ and IL-1β in the colon were also not observed in BL-fed mice treated with anti-CD4 antibody (Fig. 4I). Consistently, BL failed to reduced *C. rodentium* loads in feces and liver in mice treated with anti-CD4 antibody (Fig. 4J and K). Together, these results demonstrate that $CD4^+$ T cells play a crucial role in modulating BL-mediated protection against *C. rodentium* infection.

#### BL prevents *C. rodentium*-induced T cell dysregulation

To investigate the effect of BL on T cell immune response, the different $CD4^+$ T cell subsets, including Th1 cells ($CD4^+IFN\text{-}\gamma^+$), Th2 cells ($CD4^+IL\text{-}4^+$), Th17 cells ($CD4^+IL\text{-}17\ A^+$) and T regulatory cells (Tregs) ($CD4^+CD25^+Foxp3^+$), were analyzed by flow cytometry (Figure S4 and Figure S5). Compared to control uninfected mice, *C. rodentium* infection led to significant expansion of $CD4^+IFN\text{-}\gamma^+$ T cells in mesenteric lymph nodes ($P = 0.016$), which was attenuated by BL ($P = 0.017$) (Fig. 5A and B). Consistently, the population of $CD4^+IFN\text{-}\gamma^+$ T cells in the spleen was also significantly increased in *C. rodentium*-infected mice ($P < 0.001$), but was reduced in mice fed with BL ($P < 0.01$) (Fig. 5F and G). However, there was no significant difference in percentage of Th2, Th17, and Tregs between CD + *C. rodentium* and BL + *C. rodentium* groups (Fig. 5C-E and H-J). Collectively, these data demonstrate that BL attenuates Th1 immune response, which corresponds with attenuated inflammation and intestinal pathology in *C. rodentium*-infected mice.

#### BL protects against gut dysbiosis in *C. rodentium*-infected mice

The gut microbiota plays an essential role in resistance and clearance of *C. rodentium* [22, 23]. To explore the modulatory effect of BL on the gut microbiota, fecal bacterial composition was evaluated utilizing Illumina

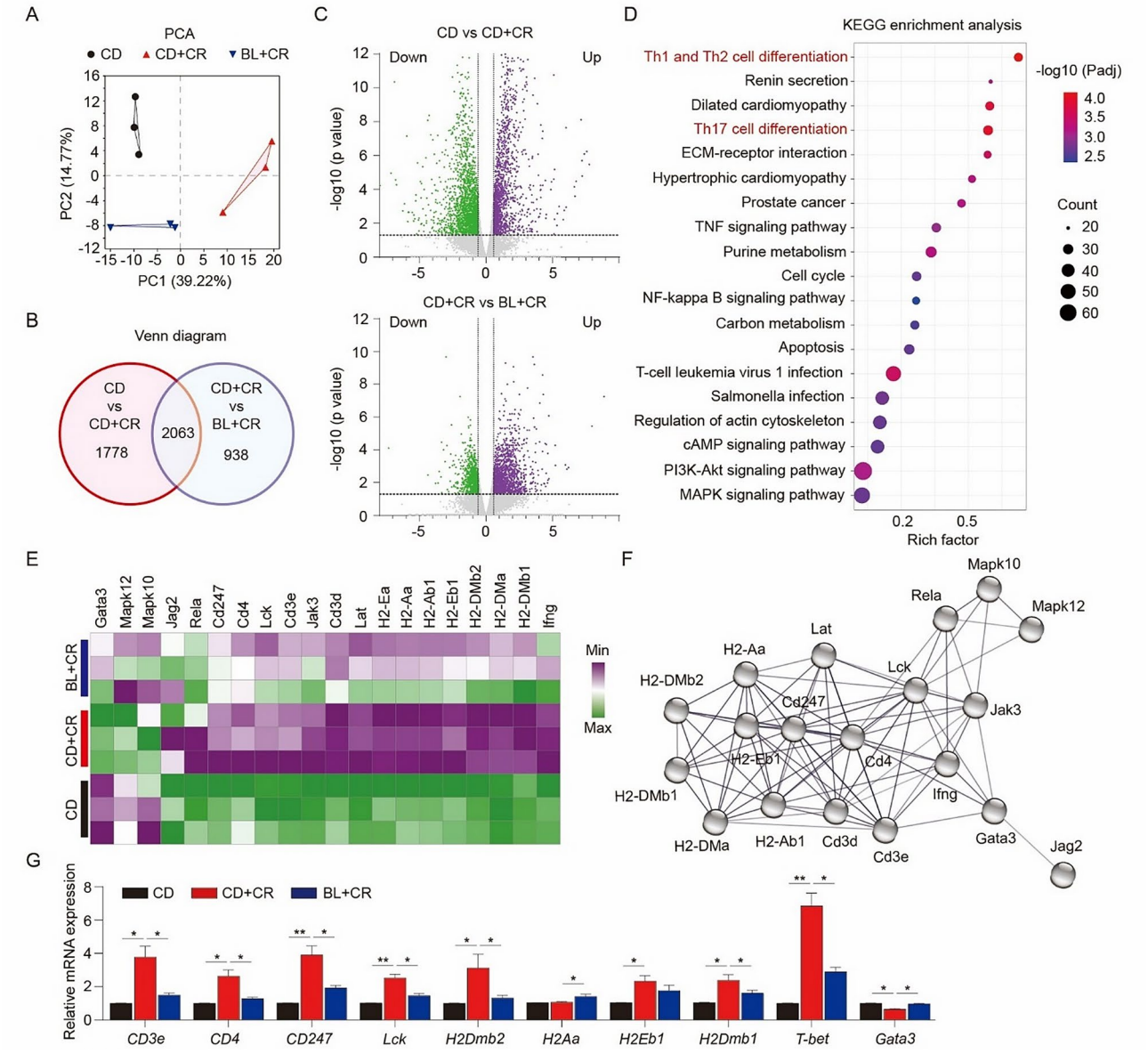


**Fig. 3** RNA sequencing analysis of the gene expression profiles in colonic tissues. (**A**) Principle component analysis (PCA) of transcriptional profiling. (**B**) Venn analysis of the differentially expressed genes (DEGs). (**C**) Volcano plot of the DEGs. (**D**) Kyoto Encyclopedia of Genes and Genomes (KEGG) pathway enrichment analysis of DEGs. (**E**) Heat map of DEGs in Th1/Th2 cell differentiation signaling pathway. Genes with fold changes of > 1.5 and P adjust (Padj) of < 0.05 were considered to be differentially expressed. (**F**) Search tool for recurring instances of neighboring genes (STRING) network visualization of the DEGs in the Th1/Th2 cell differentiation signaling pathway. (**G**) Real-time PCR assay for the DEGs in Th1/Th2 cell differentiation signaling pathway ($n = 6$ per group). Data are mean ± SEM. $^{*}P < 0.05$ and $^{**}P < 0.01$. Statistical analysis was performed using one-way analysis of variance (ANOVA) followed by Tukey's multiple comparison's test

sequencing of the V3-V4 region of 16 S rRNA genes. Alpha diversity analysis with Chao1 and Shannon index showed that *C. rodentium* treatment led to a reduction in gut microbial richness and diversity, which was abolished by BL supplementation (Fig. 6A and B). Partial Least Squares Discriminant Analysis (PLS-DA) of the microbial community showed that there were distinct group-based clustering patterns among the different treatment groups (Fig. 6C). The abundances of predominant phyla and genus were further compared. At the phylum level, the relative abundance of Proteobacteria was increased in *C. rodentium*-infected mice and was reduced with BL supplementation (Fig. 6D; Figure S6). Further, we observed an overgrowth of *Citrobacter* in *C. rodentium*-infected mice, whereas the relative abundance of *Lactobacillus* was increased in *C. rodentium*-infected mice fed with BL (Fig. 6E; Figure S6). Correspondingly, Wilcoxon rank-sum test confirmed that BL supplementation

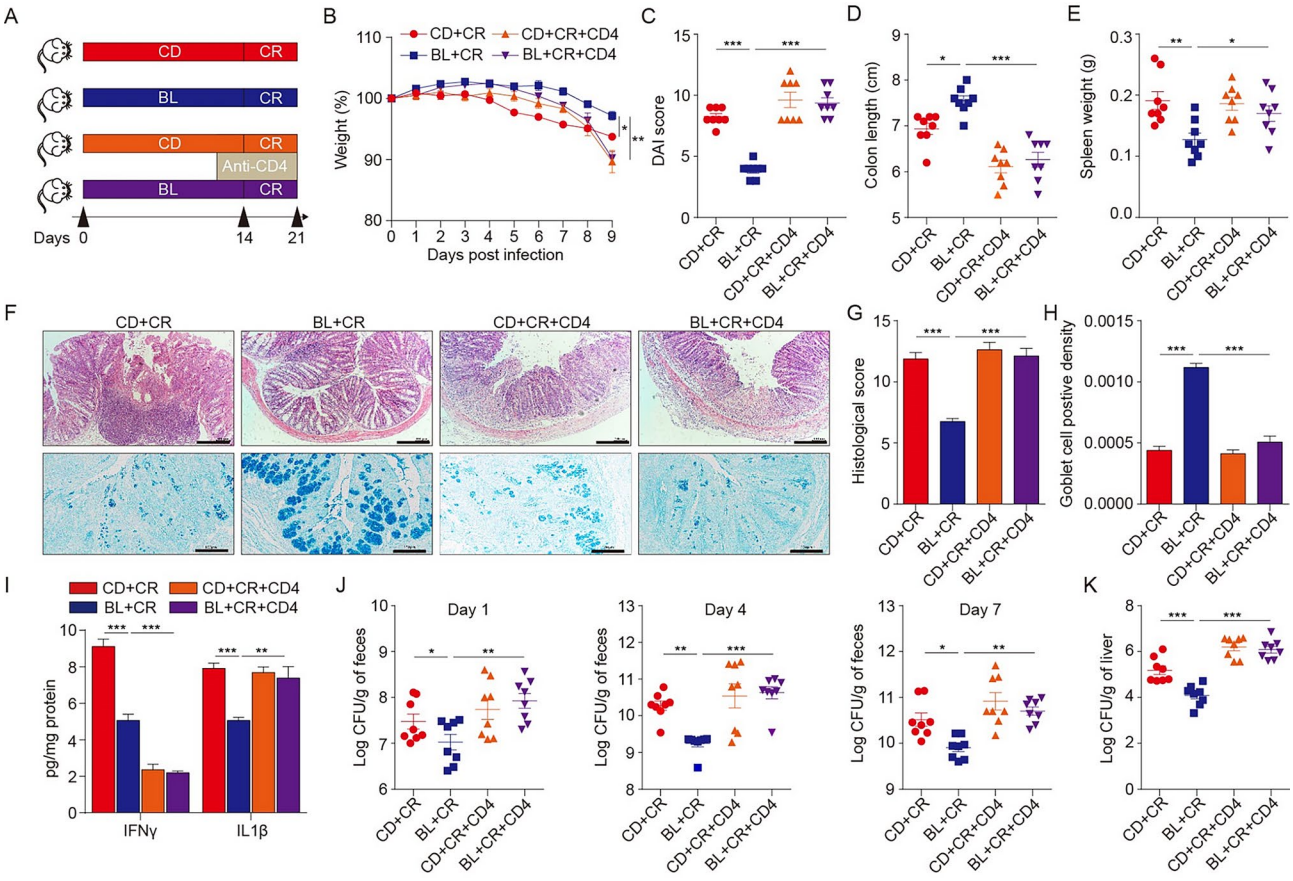


**Fig. 4** Barley leaf (BL) protects against *C. rodentium* (CR)-induced colitis in a $CD4^+$ T cell-dependent manner. (**A**) Study design of in vivo mouse experiment. Mice were fed with a standard chow diet (CD) or an isocaloric BL-supplemented diet for 2 weeks prior to the infection with CR for 10 days. For clearance of $CD4^+$ T cells, mice were injected intraperitoneally with an anti-CD4 monoclonal antibody or its isotype control antibody once every three days at 500 μg each time for three times before and during CR infection. (**B**) Body weight change. (**C**) Disease activity index (DAI) scores. (**D**) Colon length. (**E**) Spleen weight. (**F**) Representative hematoxylin and eosin (H&E) staining images of colon tissues. Scale bar, 100 μm. Representative images of alcian blue-stained colonic sections. Scale bar, 100 μm. (**G**) Histological scores. (**H**) Quantification of mucusproducing goblet cells. (**I**) The levels of IFN-γ, IL-1β, and TNF-α in the colon. (**J**) Number of CR in feces on days 1, 4, and 7 post-infection. (**K**) Number of CR in liver on day 7 post-infection. $n = 8$ per group. Data are mean ± SEM. $^*P < 0.05$, $^{**}P < 0.01$ and $^{***}P < 0.001$. For body weight change, a repeated measure two-way analysis of variance (ANOVA) was performed and the rest of the statistics were performed with one-way ANOVA followed by Tukey's multiple comparison's test

induced a significant increase in bacteria belonging to the *Lactobacillus* genus in both *C. rodentium*-infected ($P < 0.05$) or -uninfected ($P < 0.05$) mice (Fig. 6F).

Next, spearman correlation analysis was performed to identify the bacteria that was responsible for BL-mediated protection against *C. rodentium* enteric infection. We found that *Lactobacillus* showed strong negative correlations with DAI, IL-1β, TNF-α, and histological score; while *Citrobacter* displayed a strong positive association with these pathologic parameters (Fig. 6G). We next assessed whether the impact of BL on gut microbiota was associated with changes in the $CD4^+IFN\text{-}\gamma^+$ T cells during *C. rodentium* infection. We found that the population of $CD4^+IFN\text{-}\gamma^+$ T cells was positively correlated with *Citrobacter* and negatively correlated with *Lactobacillus* (Figure S7).

Short-chain fatty acids (SCFAs) serve as critical microbial metabolites of SCFAs-producing bacteria such as *Lactobacillus* in modulating the gut homeostasis [31–34]. We found that the fecal levels of acetate, propionate, butyrate, isobutyrate, valerate, and isovalerate were reduced in *C. rodentium*-infected mice compared to control uninfected mice. However, the levels of SCFAs, which were negatively correlated with colitis-related indexes, were significantly elevated in BL-fed mice (Fig. 6H; Figure S8). Together, these findings suggest that the protective effect of BL against *C. rodentium*-induced immune dysregulation is closely linked to improvement of gut microbiota dysbiosis.

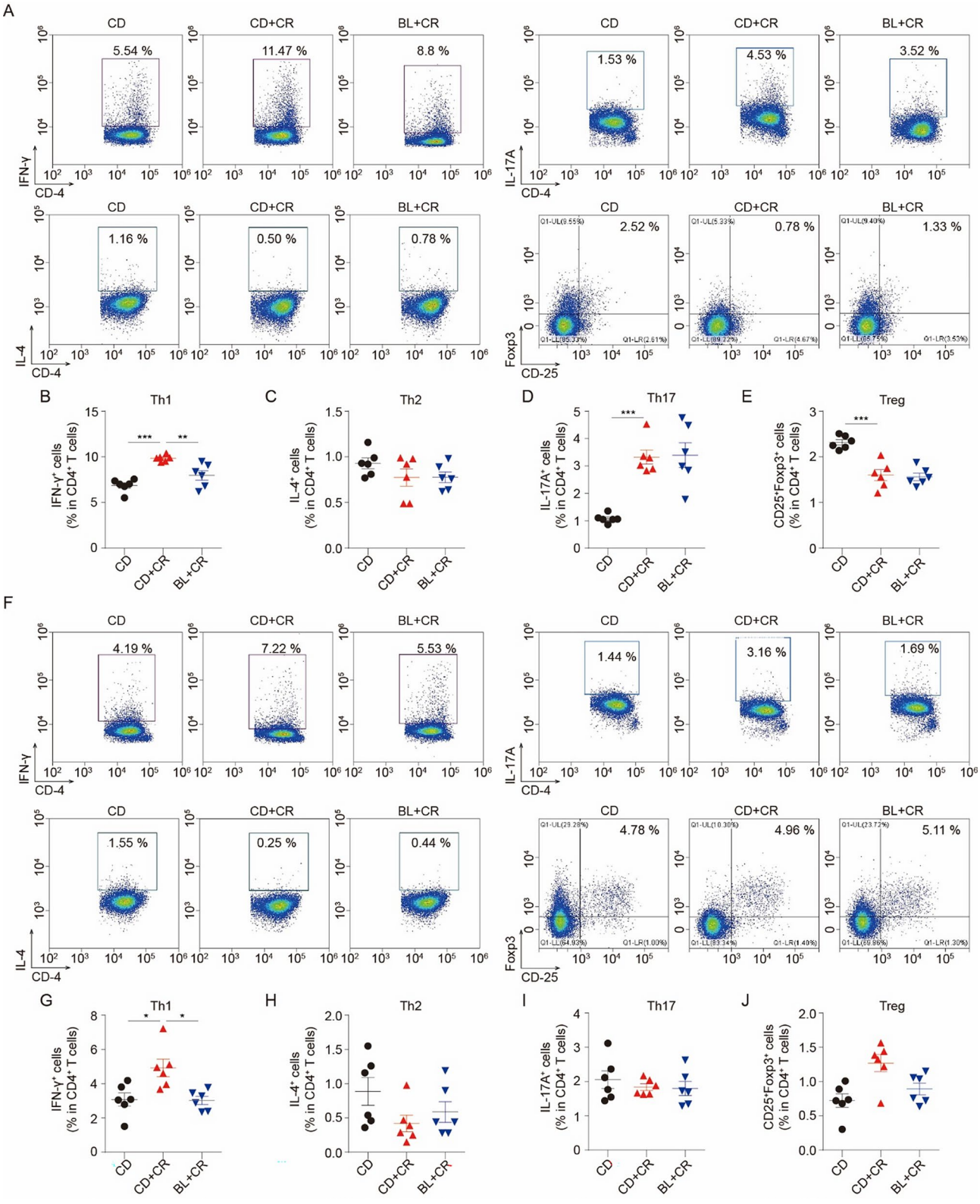


**Fig. 5** (See legend on next page.)

(See figure on previous page.)

**Fig. 5** Flow cytometric analysis of $CD4^+$ T cell subsets in mouse mesenteric lymph node and spleen. (**A**) Representative flow cytometry profile of $CD4^+IFN\text{-}\gamma^+$ cells, $CD4^+IL\text{-}4^+$ cells, $CD4^+IL\text{-}17\ A^+$ cells and $CD4^+CD25^+Foxp3^+$ cells in mouse mesenteric lymph node. (**B**) Quantification of $CD4^+IFN\text{-}\gamma^+$ cells. (**C**) Quantification of $CD4^+IL\text{-}4^+$ cells. (**D**) Quantification of $CD4^+IL\text{-}17\ A^+$ cells. (**E**) Quantification of $CD4^+CD25^+Foxp3^+$ cells. (**F**) Representative flow cytometry profile of $CD4^+IFN\text{-}\gamma^+$ cells, $CD4^+IL\text{-}4^+$ cells, $CD4^+IL\text{-}17\ A^+$ cells and $CD4^+CD25^+Foxp3^+$ cells in mouse colon. (**G**) Quantification of $CD4^+IFN\text{-}\gamma^+$ cells. (**H**) Quantification of $CD4^+IL\text{-}4^+$ cells. (**I**) Quantification of $CD4^+IL\text{-}17\ A^+$ cells. (**J**) Quantification of $CD4^+CD25^+Foxp3^+$ cells. $n = 6$ per group. Data are mean ± SEM. $^{**}P < 0.01$ and $^{***}P < 0.001$. Statistical analysis was performed using one-way analysis of variance (ANOVA) followed by Tukey's multiple comparison's test

### Gut microbiota confers protection of BL against *C. rodentium*-induced enteric infection

To further confirm the role of gut microbiota in the protective effects of BL against *C. rodentium*, fecal microbiota transplantation (FMT) was performed (Fig. 7A). In this study, antibiotic treatment was used to deplete the gut microbes and the antibiotic-treated recipient mice were then gavaged with the mixture of stool pellets from donor mice during the FMT (Fig. 7A). 16 S rRNA sequencing was used to determine whether the gut microbiota of donor mice was successfully transplanted into the recipient mice (Figure S9). Our result revealed clear discrimination between the FMT-treated two groups (Figure S9). Importantly, there is a high similarity in the gut microbiota community between the donor and the corresponding recipient mice (Figure S9). Consistent with our previous results, mice that received microbiota from BL-fed mice displayed an increased abundance of *Lactobacillus* compared with control recipient mice (Fig. 7B).

We further studied the functional significance of BL-mediated gut microbiome in the modulation of host response to *C. rodentium* infection. We found that mice received microbiota from BL-fed mice showed attenuated body weight loss and reduced DAI score compared to mice received microbiota from control CD-fed mice (Fig. 7C and D). Moreover, a longer colon length and a lower spleen weight were detected in mice received microbiota from BL-fed mice compared to mice received microbiota from control mice (Fig. 7E and F). Histological analysis of colon tissues revealed that mice received microbiota from BL-fed mice exhibited attenuated tissue damage and alleviated goblet cell depletion compared to control recipient mice (Fig. 7G-I). The severity of inflammation was improved in recipient mice that were colonized by BL-induced microbiota, as evidenced by reduced levels of IFN-γ and IL-1β in colonic tissues (Fig. 7J). Correspondingly, the bacterial level of *C. rodentium* in feces, spleen, and liver was reduced in mice received microbiota from BL-fed mice compared to control recipient mice (Fig. 7K-M). Collectively, these results confirm the crucial role of gut microbiota in protective effect of BL against *C. rodentium* infection.

### *L. plantarum* attenuates *C. rodentium* infection-induced colonic inflammation

*Lactobacillus* was identified as the most enriched genus in BL-fed mice and mice received microbiota from BL-fed mice (Fig. 6F and Fig. 7B). By using real-time polymerase chain reaction (PCR), 9 common *Lactobacillus* strains *L. rhamnosus*, *L. brevis*, *L. murinus*, *L. fermentum*, *L. reuteri*, *L. delbrueckii*, *L. casei*, *L. salivarius*, and *L. plantarum* in the genome of the intestinal microbiota were quantified. Notably, *L. plantarum* was the only species that significantly enriched in BL-fed mice compared to the control CD-fed mice (Figure S10A). We hypothesized that BL may act as a prebiotic to enrich the commensal bacterium *L. plantarum* and assessed the direct effects of BL on *L. plantarum* growth. We found that the growth of *L. plantarum* was significantly promoted by BL treatment (Figure S10B). These data indicate that *L. plantarum* may play a beneficial role in alleviating *C. rodentium*-associated pathology.

To investigate the role of *L. plantarum* in *C. rodentium*-induced colitis, we administered phosphate-buffered saline (PBS), live *L. plantarum* or heat-inactivated *L. plantarum* to *C. rodentium*-infected mice (Fig. 8A). The qPCR analysis confirmed that administration of live *L. plantarum* resulted in increased abundance of *L. plantarum* in mouse feces (Fig. 8B). We found that mice administered with *L. plantarum* has significantly attenuated manifestations of colitis compared to mice gavaged with PBS, as demonstrated by body weight loss and DAI score (Fig. 8C and D). Although *L. plantarum* had no impact on the spleen weight, the colon length was significantly longer in mice administered with *L. plantarum* compared to mice gavaged with PBS (Fig. 8E and F). Histological analysis revealed that *C. rodentium*-induced pathological damage and mucosal barrier dysfunction were also abrogated by *L. plantarum* (Fig. 8G-I). The colonic expression of *Sla26a3* and *Car4* was increased and *T-bet* expression was reduced in mice received *L. plantarum* administration (Fig. 8J and K). Furthermore, *C. rodentium* infection led to elevated levels of *C. rodentium* in feces, liver, and cecum, which were significantly reduced by *L. plantarum* (Fig. 8L-N). Notably, heat-inactivated *L. plantarum* failed to confer the above beneficial effects on *C. rodentium* infection (Fig. 8C-N). Collectively, these results indicate that *L. plantarum* enriched with BL supplementation plays a crucial role in protection against *C. rodentium*-induced intestinal inflammation.

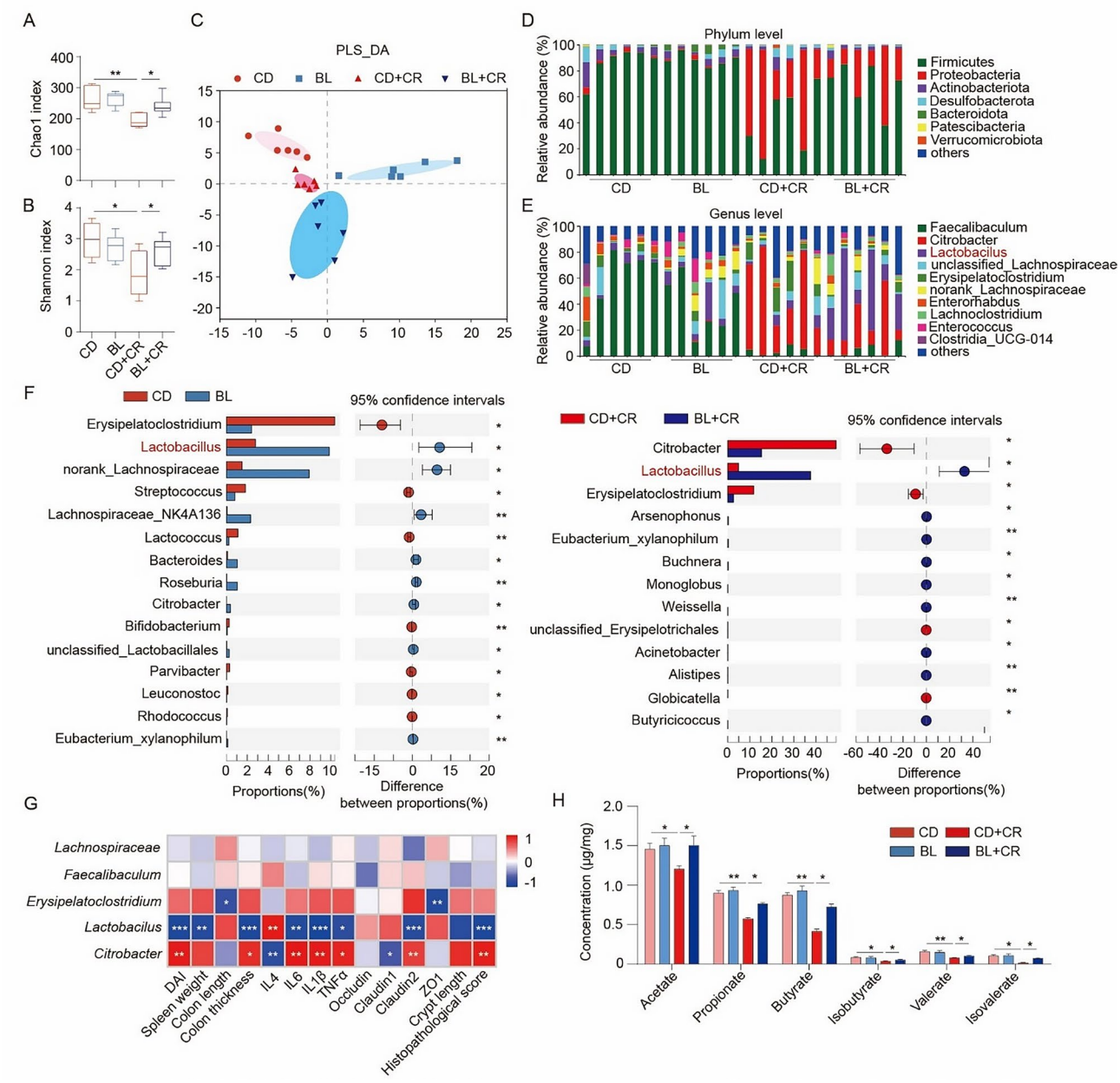


**Fig. 6** Barley leaf (BL) prevents *C. rodentium* (CR)-induced gut microbiota dysbiosis. (**A**) Chao1 index. (**B**) Shannon index. (**C**) Partial least squares-discriminant analysis (PLS-DA) score plots of the gut microbiota composition. (**D**) Taxonomic distributions of gut bacterial composition at the phylum level. (**E**) Taxonomic distributions of gut bacterial composition at the genus level. (**F**) Comparison of gut bacterial composition at the genus level. (**G**) Spearman correlations analysis between the gut bacteria and colitis-related indexes. (**H**) Concentrations of short-chain fatty acids in feces. In (**A**) - (**G**), ($n=6$ per group). In (**H**), ($n=8$ per group). Data are mean ± SEM. *$P<0.05$, **$P<0.01$ and ***$P<0.001$. For (**F**), statistical analysis was performed using a two-tailed Wilcoxon rank-sum test by R Project. For (**G**), a statistically significant correlation was performed using linear regression analyses. The rest of the statistics were performed using a one-way analysis of variance (ANOVA) followed by Tukey's multiple comparison's test

### *L. plantarum* ameliorates *C. rodentium*-induced colitis through its secreted EVs

Bacterial EVs are membrane-enclosed lipid bilayer nanoparticles that play essential roles in communication between gut microbiome and human health [35]. Recently, the EVs derived from probiotics particularly *Lactobacillus* have emerged as potential mediators of host immune response and anti-inflammatory effect [35].

However, the role of *L. plantarum*-derived EVs (L-EVs) in *C. rodentium* infection and intestinal inflammation remains unclear. We thus isolated EVs from the supernatants of *L. plantarum* using an ultracentrifugation-based system (Fig. 9A). The scanning electron microscopy

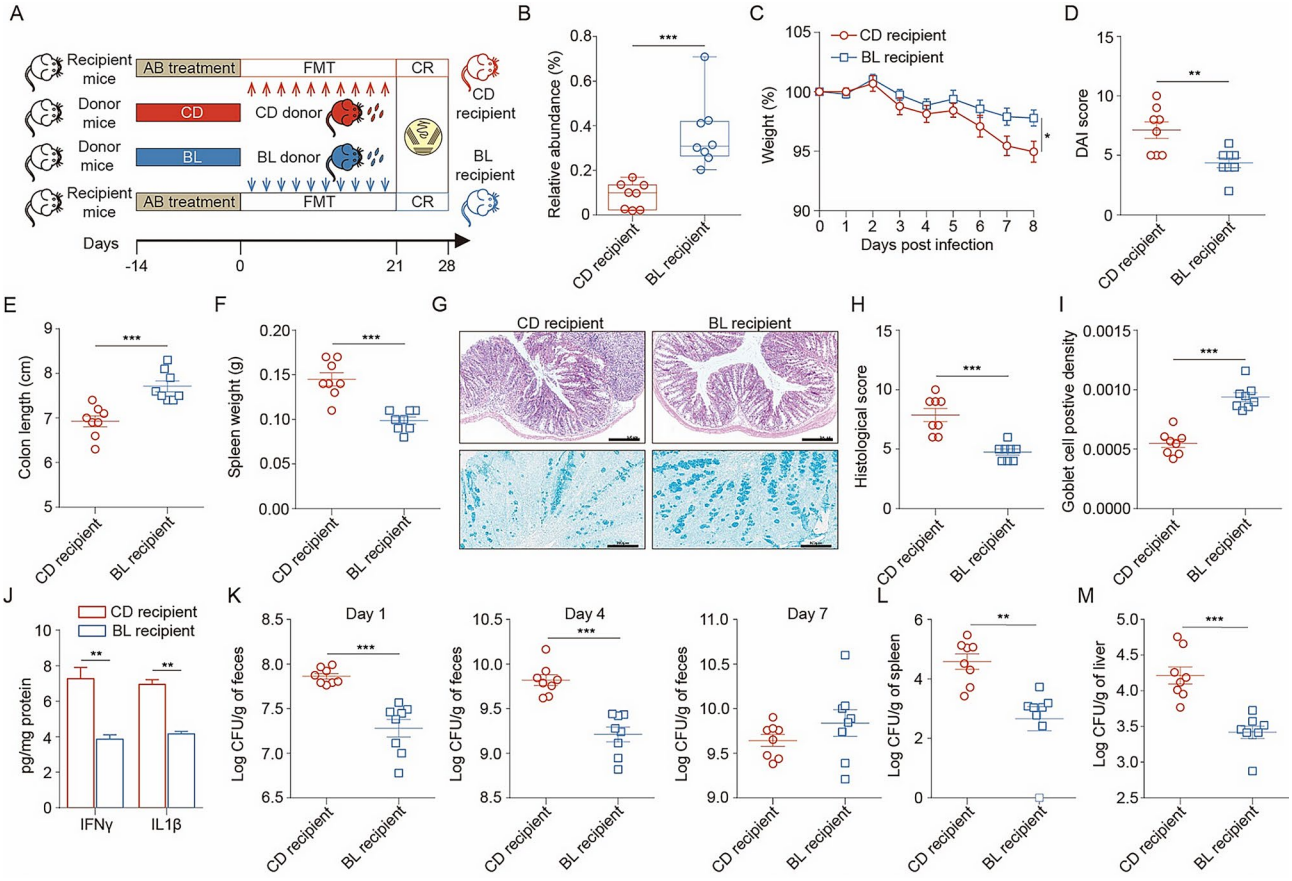


**Fig. 7** Transplantation of feces from barley leaf (BL)-fed mice protects against *C. rodentium* (CR)-induced colitis. (**A**) Study design of in vivo mouse fecal microbiota transplantation (FMT) experiment. The recipient mice received a two-week treatment of combined antibiotics (neomycin, penicillin, metronidazole, 1000 mg/l; vancomycin and streptomycin 500 mg/l) before FMT to remove the native microbiota. The donor mice were fed a standard chow diet (CD) or an isocaloric BL-supplemented diet for 2 weeks. Fresh feces from donor mice were collected and resuspended in sterile PBS at 1:10 (m/v), vortexed, and rested, then the supernatant was taken for transplantation for three weeks. (**B**) Body weight change. (**C**) Disease activity index (DAI) scores. (**D**) Colon length. (**E**) Spleen weight. (**F**) Representative hematoxylin and eosin (H&E) staining images of colon tissues. Scale bar, 100 μm. Representative images of alcian blue-stained colonic sections. Scale bar, 100 μm. (**G**) Histological scores. (**H**) Quantification of mucusproducing goblet cells. (**I**) The levels of IFN-γ, IL-1β, and TNF-α in the colon. (**J**) Number of CR in feces on days 1, 4, and 7 post-infection. (**K**) Number of CR in the spleen on day 7 post-infection. (**L**) Number of CR in the liver on day 7 post-infection. $n = 8$ per group. Data are mean ± SEM. $^{*}P < 0.05$, $^{**}P < 0.01$ and $^{***}P < 0.001$. For body weight change, a repeated measure two-way analysis of variance (ANOVA) was performed and the rest of the statistics were performed with Student's t-test

and transmission electron microscopy showed that the isolated L-EVs were double-layer membrane-enclosed nanoparticles with spherical morphology (Fig. 9B and C). The nanoparticle tracking analysis (NTA) analysis showed that the mean particle size of L-EVs ranged from 100 nm to 200 nm in diameter (Fig. 9D), which was consistent with the size of previous reports [35]. We further performed proteomic analysis to characterize the protein composition of L-EVs. A total of 380 proteins were identified to be present in L-EVs. The biological functions of these proteins were analyzed by using the Gene Ontology (GO) database. The top ranked proteins are localized to the plasma membrane (26.61%), suggesting that L-EVs might originate directly from the budding of plasma membrane. KEGG pathway enrichment analysis further indicated that L-EVs-enriched proteins were primarily associated with amino acid metabolism, energy metabolism, antimicrobial and infectious disease. Specifically, most of them were found to be significantly involved in the modulation of signal peptide, or via JAK/STAT pathway, NF-κB pathway and TLR pathway [36–39].

We evaluated the biosafety of L-EVs. There is no notable difference in daily food intake, body weight changes, and weight of organs (colon, liver, and spleen) between the L-EVs group and the control group (Figure S11A-E). Histological analysis showed that oral administration of L-EVs at the different dose did not cause any colon, liver, and spleen damage (Figure S11F). Furthermore, cytokine profiling analysis indicated no significant difference in serum levels of IFN-γ and TNF-α (Figure S11G and H). In addition, we supplemented in vivo studies with DiR-labeled L-EVs and demonstrated that these vesicles remain stable in circulation and effectively reach and

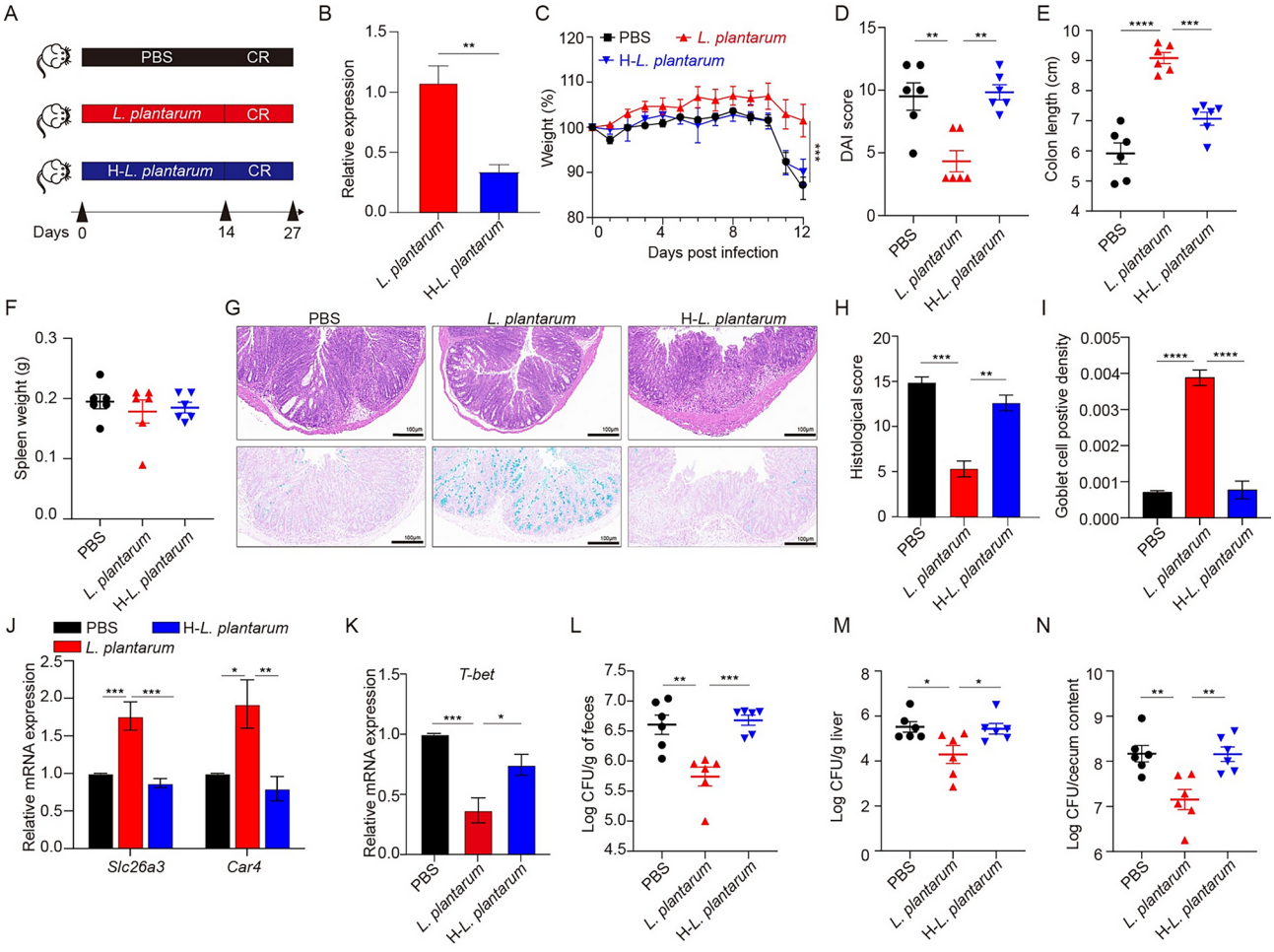


**Fig. 8** *Lactobacillus plantarum* (*L. plantarum*) attenuates colonic inflammation in *C. rodentium* (CR)-infected mice. (**A**) Study design of in vivo mouse experiment. Mice were gavaged daily with phosphate-buffered saline (PBS), $10^9$ CFU of live *L. plantarum* or $10^9$ CFU of heat-inactivated *L. plantarum* (H-*L. plantarum*) for 2 weeks prior to the infection with CR for 12 days. (**B**) Real-time polymerase chain reaction (PCR) assay for the quantification of *L. plantarum* in mouse feces. (**C**) Body weight change. (**D**) Disease activity index (DAI) scores. (**E**) Colon length. (**F**) Spleen weight. (**G**) Representative hematoxylin and eosin (H&E) staining images of colon tissues. Scale bar, 100 μm. Representative images of alcian blue-stained colonic sections. Scale bar, 100 μm. (**H**) Histological scores. (**I**) Quantification of mucusproducing goblet cells. (**J**) Real-time PCR assay for the expression of *T-bet* in the colon. (**K**) Real-time PCR assay for the expression of *Slc26a3* and *Car4* in the colon. (**L**) Number of CR in feces on days 1 post-infection. (M) Number of CR in liver on day 1 post-infection. (**N**) Number of CR in cecum content on day 1 post-infection. $n = 6$ per group. Data are Mean ± SEM. $^*P < 0.05$, $^{**}P < 0.01$ and $^{***}P < 0.001$. For (**B**), Student's *t*-test was performed. For (**C**), a repeated measure two-way analysis of variance (ANOVA) was performed and the rest of the statistics were performed with one-way ANOVA followed by Tukey's multiple comparison's test

persist in the colon without significant off-target distribution (Figure S12). These results suggest that L-EVs exhibit favourable stability and safety profiles.

To investigate whether the beneficial effects of *L. plantarum* were associated with their secreted EVs, L-EVs were administered to mice by oral gavage followed by the infection with *C. rodentium* (Fig. 10A). Our results showed that the dramatic loss of body weight and increased DAI score in *C. rodentium*-infected mice were significantly reduced by L-EVs intervention (Fig. 10B and C). Moreover, L-EVs mitigated *C. rodentium*-induced colon length shortening and increased spleen weight (Fig. 10D and E). Histopathological analysis showed that *C. rodentium*-induced increase in pathology score and mucosal barrier injury could be alleviated by L-EVs treatment (Fig. 10F-H). Similar trends were obtained with the expression of *Ifnγ*, *Tnfα*, *Sla26a3* and *Car4* in colon tissues (Fig. 10I and J). The *C. rodentium* loads in feces, liver, and cecum were significantly reduced in L-EVs-treated mice (Fig. 10K-M). We then further analyzed the population of $CD4^+$ T cells. The increased population of $CD4^+IFN\text{-}\gamma^+$ T cells in the spleen was significantly reduced by L-EVs intervention (Fig. 10N and O). Collectively, these results suggest that *L. plantarum* attenuates *C. rodentium* infection and intestinal inflammation via its secreted EVs.

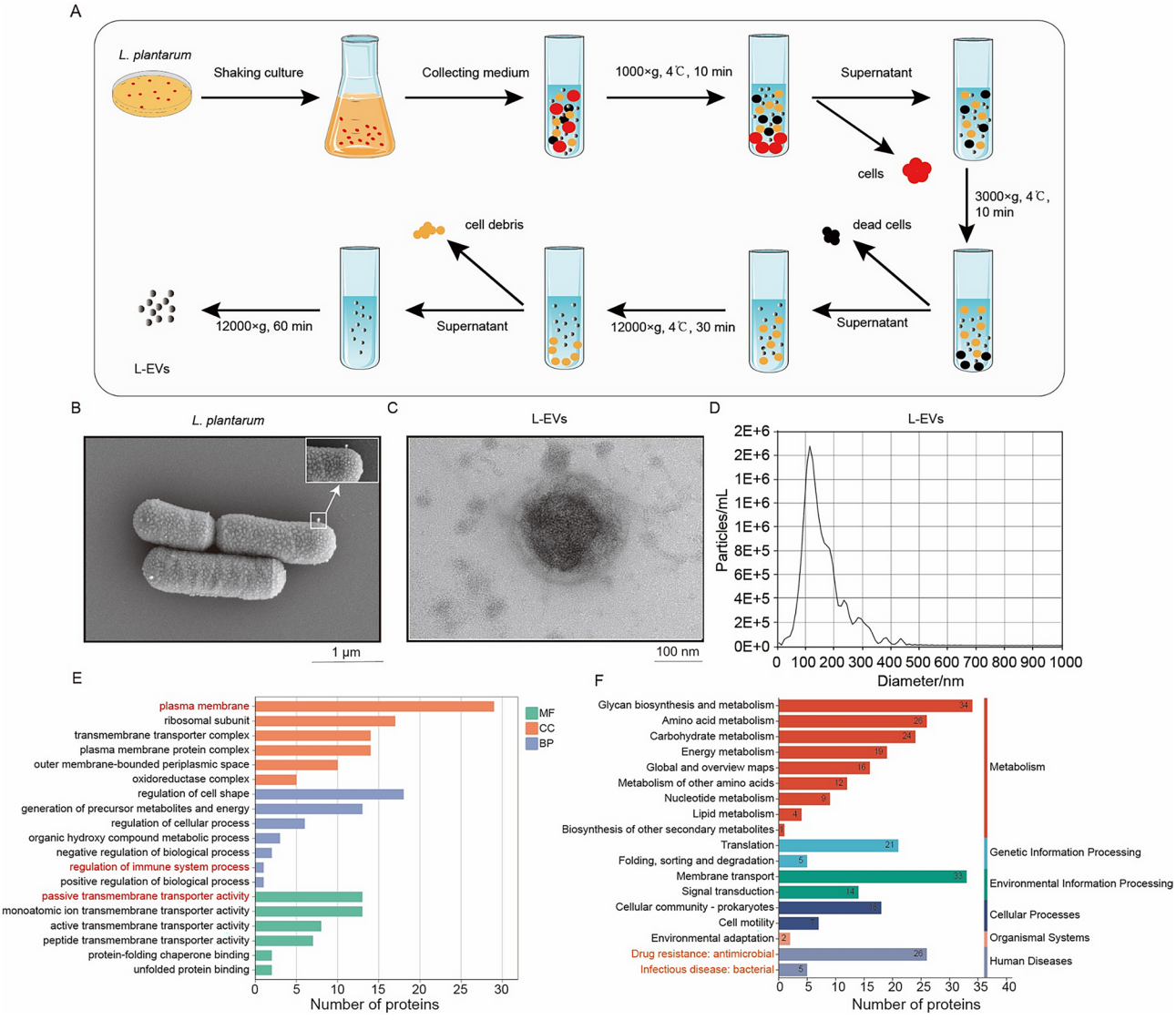


**Fig. 9** Preparation and characterization of *L. plantarum*-derived EVs (L-EVs). (**A**) Isolation and purification procedures of L-EVs. (**B**) Representative image of the scanning electron microscope for *L. plantarum* showing membrane vesicles on the bacterial cell surface. (**C**) Representative image of the transmission electron microscopy for L-EVs. (**D**) Nanoparticle tracking analysis was performed to detect the size distribution of L-EVs. (**E**) Go secondary classification statistical charts of L-EVs. (**F**) KEGG annotated statistical charts of L-EVs

## Discussion

The impacts of global increase in the prevalence of IBD on human public health are fundamental and challenging [4]. The pathogenesis of IBD is thought to associate with the dysregulated interplay between environmental changes, gut microbiota, and host immune response [9]. Invasion by pathogenic microbes is an important source of factor contributing to infectious diarrhea and colitis. Although our previous studies have shown that BL is effective in protecting against chemically-induced intestinal damage [28–30], the potential benefits of BL on enteropathogenic infection and intestinal inflammation is unclear. In this study, the mechanism underlying the protective effects of BL against *C. rodentium* infection and colitis was studied.

The BL dosage used in this study is a human equivalent dose that has been reported without adverse effects [40]. Our results showed that dietary supplementation with BL alleviated *C. rodentium*-induced gut barrier impairment and pro-inflammatory Th1 immune response. The protective effects of BL were associated with improvement of gut microbiota dysbiosis and enrichment of *Lactobacillus*. More significantly, our results demonstrated for the first time that EVs secreted by *L. plantarum* act as an important mediator of the protection against *C. rodentium*-induced bacterial colitis and suppression of host Th1 immune response dysregulation. Therefore,

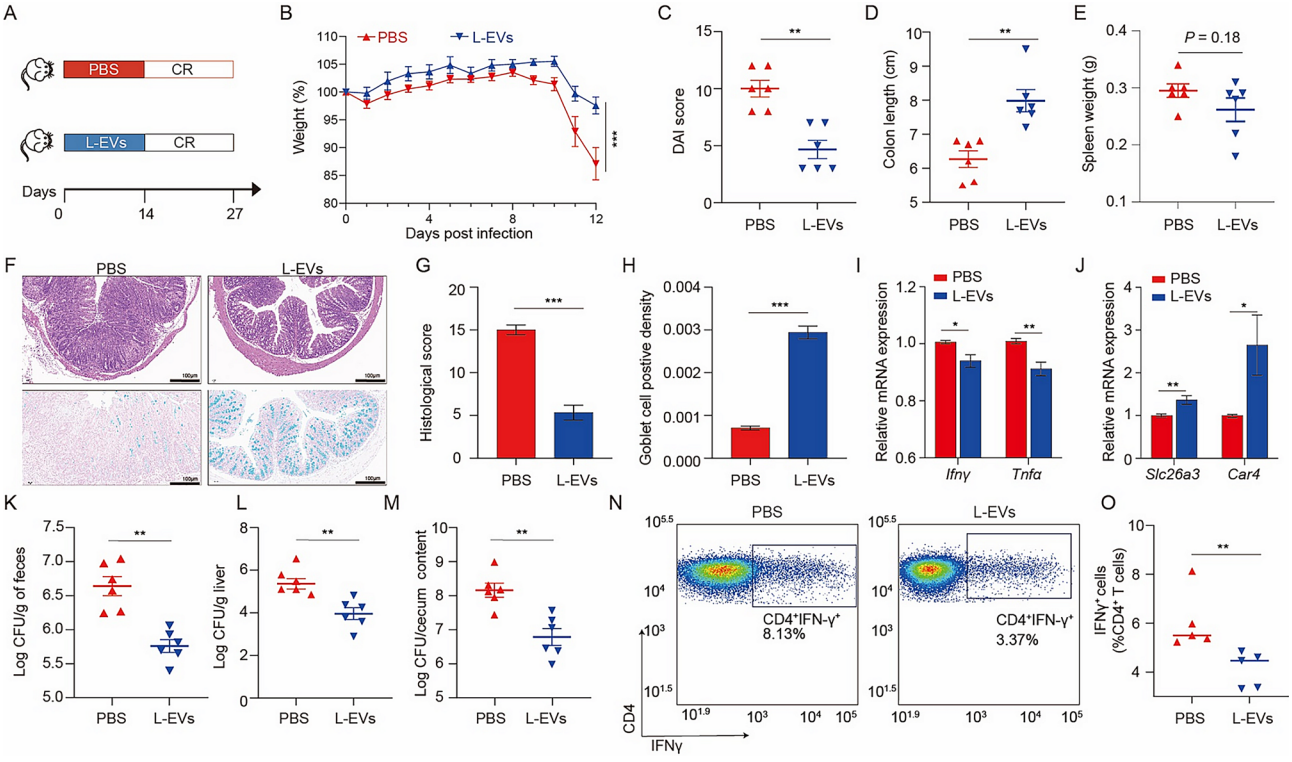


**Fig. 10** *L. plantarum*-derived EVs (L-EVs) ameliorates *C. rodentium* (CR)-induced colitis. (**A**) Study design of in vivo mouse experiment. Mice were gavaged daily with phosphate-buffered saline (PBS) or 50 μg of L-EVs for 2 weeks prior to the infection with CR for 12 days. (**B**) Body weight change. (**C**) Disease activity index (DAI) scores. (**D**) Colon length. (**E**) Spleen weight. (**F**) Representative hematoxylin and eosin (H&E) staining images of colon tissues. Scale bar, 100 μm. Representative images of alcian blue-stained colonic sections. Scale bar, 100 μm. (**G**) Histological scores. (**H**) Quantification of mucusproducing goblet cells. (**I**) Real-time PCR assay for the expression of *Ifnγ*and *Tnfa* in the colon. (**J**) Real-time PCR assay for the expression of *Slc26a3* and *Car4* in the colon. (**K**) Number of CR in feces on days 1 post-infection. (**L**) Number of CR in liver on day 1 post-infection. (**M**) Number of CR in cecum content on day 1 post-infection. (**N**) Representative flow cytometry profile of $CD4^+IFN\text{-}\gamma^+$ cells. (**O**) Quantification of $CD4^+IFN\text{-}\gamma^+$ cells. $n = 5$–6 per group. Data are Mean ± SEM. $^*P < 0.05$, $^{**}P < 0.01$ and $^{***}P < 0.001$. For (**B**), a repeated measure two-way analysis of variance (ANOVA) was performed and the rest of the statistics were performed Student's *t*-test

these results shed light on the potential use of BL and probiotic-derived EVs for the clinical management of infection-associated intestinal inflammatory disorders in humans.

We found that mice infected with *C. rodentium* developed severe colitis manifestations including weight loss, colon shortening, and spleen hyperplasia, which are consistent with previous studies [14, 17]. The deleterious effects caused by *C. rodentium* infection were attenuated in BL-fed mice. Crypt hyperplasia, which is characterized by an overproliferation of undifferentiated $Ki67^+$ cells, is an important hallmark of *C. rodentium*-induced infection [14, 17]. The induction of colonic crypt hyperplasia is a mechanism by which *C. rodentium* facilitates aerobic respiration to compete with the gut microbiota during infection [41]. This process is regulated by the T3SS, which plays a central role in determining the colonization efficiency of *C. rodentium* [41]. In this study, we observed that *C. rodentium*-induced increase in the number of colonic $Ki67^+$ cells was abrogated in BL-fed mice. Moreover, the bacterial loads of *C. rodentium* in feces and cecum contents were reduced in BL-fed mice compared to the control mice. This was accompanied by a low expression level of T3SS-associated virulence factors (*Tir*, *Map*, and *EspA*) in the colon and cecum of BL-fed mice. Thus, our data suggest that BL alleviates *C. rodentium* infection by limiting the bacterial colonization and mitigating colonic crypt hyperplasia.

The intestinal epithelial barrier, which composes of a single layer of epithelial cells through the tight junction and adhesion proteins, serves as a defensive system involving host-microbial interaction and intestinal homeostasis [42]. The colonic goblet cells secret MUC2 to form a mucus layer, which is a key defense against enteric pathogens [43]. In this study, we found that *C. rodentium* infection caused a reduction of mucus-producing goblet cells in the colon, which was effectively ameliorated by BL intervention. The mRNA expression of tight junction proteins and adhesion junctions (*Occludin*, *Claudin1*, and *ZO-1*) as well as chloride anion exchanger and water absorption proteins (*Sla26a3* and *Car4*) [44] was restored in *C. rodentium*-infected mice fed with BL.

These results may partially explain the reduced bacterial loads of *C. rodentium* in the spleen and liver of BL-fed mice and suggest that BL prevents the extraintestinal transmission of *C. rodentium* by improving the gut barrier function.

A finely tuned inflammatory response is necessary to defend against *C. rodentium*-induced infection by enhancing gut barrier and limiting bacterial translocation [18]. However, uncontrolled or prolonged inflammatory response may lead to intestinal barrier impairment and increased risk of infection complications. Here, we found that *C. rodentium* infection induced a robust inflammatory response characterized by the increased production of inflammatory cytokines including TNF-α, IFN-γ, and IL-1β; meanwhile, the expression level of macrophage marker F4/80 in colonic tissue was elevated in mice infected with *C. rodentium*. BL effectively dampened the increased expression levels of TNF-α, IFN-γ, and IL-1β. Thus, the reduced bacterial loads and improved gut barrier function in BL-fed mice may be due to the attenuation of *C. rodentium*-induced inflammatory responses.

We next used RNA sequencing to investigate the mechanisms underlying the anti-inflammatory effects of BL against *C. rodentium* infection. Intriguingly, functional analysis showed that the pathways of Th1/Th2 and Th17 cell differentiation were significantly enriched in BL-fed mice. As the major producers of inflammatory cytokines, adaptive immune $CD4^+$ T cells are essential for defending against *C. rodentium* infection [19, 20]. It is reported that $CD4^+$ T cells can be subdivided into Th1, Th2, Th17, and Tregs [45]. *C. rodentium* infection in mice elicits a Th1/Th17 response similar to those of patients with pathogenic EPEC/EHEC infections [46]. Notably, depletion of $CD4^+$ T cells by anti-CD4 antibody treatment effectively abrogated the beneficial effects of BL on *C. rodentium*-induced colitis, suggesting that $CD4^+$ T cells play a role in regulating the protection against *C. rodentium* infection. To further evaluate the impacts of BL on *C. rodentium*-induced T cell immune response, flow cytometry was used to analyze the different $CD4^+$ T cell subsets in the mesenteric lymph node and spleen. We found that *C. rodentium*-infected mice developed a considerable increase in the proportion of Th1 cells ($CD4^+IFN\text{-}\gamma^+$), which was attenuated in BL-fed mice. Notably, the proportions of Th2 cells ($CD4^+IL\text{-}4^+$), Th17 cells ($CD4^+$IL-17 $A^+$), and Treg cells ($CD4^+CD25^+Foxp3^+$) were not affected. These results indicate that BL alleviates *C. rodentium*-induced colitis at least in part by alleviating $CD4^+$ T cell dysregulation.

The gut microbiota has been known as a major regulator in pathogen-host interactions and plays a significant role in controlling the severity of *C. rodentium*-associated colon pathology [16, 17, 43]. Accumulating evidence has shown that marked variations exist in the composition of the gut microbiota between IBD patients and healthy individuals. For instance, gut microbiota dysbiosis featured by a reduction of microbial diversity was observed in patients with IBD [47, 48]. The reduced gut bacterial diversity may be due to the expansion of facultative anaerobic pathogens in Proteobacteria, such as *Salmonella*, *Escherichia coli*, and *Shigella* [49]. In line with these findings, our 16 S rRNA gene sequencing analysis showed that *C. rodentium* infection induced a decreased bacterial diversity and an increased abundance of Proteobacteria. The abundance of *Citrobacter* was elevated in *C. rodentium*-infected mice but dropped markedly in BL-fed mice, suggesting that *C. rodentium*-induced gut dysbiosis was effectively abrogated. Importantly, the beneficial effect of BL against *C. rodentium*-induced colitis was transferable via FMT, suggesting that the consumption of BL may shape a gut microenvironment that is sufficient to alleviate *C. rodentium* infection and intestinal inflammation. It is important to note that the 16 S rRNA sequencing employed in this study primarily focuses on the bacterial microbiota, and therefore does not account for other microbial groups such as fungi or viruses. Both fungi and viruses have been implicated in the modulation of gut health and inflammation, and their roles in colitis are increasingly recognized. As such, the absence of fungal and viral data is a limitation of our study. Future research incorporating more comprehensive sequencing techniques, such as metagenomics or broader 18 S rRNA sequencing, could provide a more holistic view of the microbiome and its interactions in colitis.

Further analysis revealed that BL substantially enhanced the relative abundance of *Lactobacillus* in both uninfected and infected mice. This result is consistent with our previous study showing that the in vitro anaerobic fermentation of BL with mouse feces resulted in an enrichment of *Lactobacillus* [29]. We thus assessed the effects of BL on *L. plantarum* growth. Our results showed that BL had a capacity to promote the growth of *L. plantarum*. Our previous study has shown that dietary fibers are the primary nutritional components of BL [50]. Together, these findings suggest that BL may act as a prebiotic agent to promote the growth of *L. plantarum*. Further studies are required to study the molecular mechanisms underlying the effect of BL on *L. plantarum* growth.

*Lactobacillus* is an important type of probiotic and is extensively used in dairy food. Several *Lactobacillus* species have been reported to be effective in ameliorating *C. rodentium*-induced bacterial colitis. For instance, *L. reuteri* could activate Wnt/β-catenin pathway to promote the proliferation of intestinal organoids, thereby protecting the intestinal mucosal barrier against pathogenic bacterial invasion [51]. *L. johnsonii* could regulate the endoplasmic reticulum stress signalling and attenuate

inflammatory responses in *C. rodentium*-infected mice [52]. However, little is known about the health benefits of *L. plantarum* in the context of *C. rodentium* infection. This study, to our knowledge, is the first to characterize the beneficial effects of *L. plantarum* on *C. rodentium*-induced colitis, highlighting its potential in future clinical application for IBD patients.

EVs are nano-sized, membrane-bound particles released by various cellular sources and play pivotal roles in various biological processes, such as cell-to-cell communication, tissue homeostasis and immune regulation [53]. Recently, commensal probiotic-derived EVs have emerged as important mediators of host-pathogen interactions. For instance, EVs derived from *L. johnsonii* were found to alleviate intestinal injury in ETECK88-infected mice through enhancing M2 macrophage polarization [54]. Moreover, administration of *L. reuteri* BBC3-derived EVs has been shown to mitigate lipopolysaccharide-induced intestinal inflammation in broiler chickens [55]. These findings suggest that bacterial EVs are becoming promising interventions or supplements for promoting intestinal homeostasis, due to their unique nano-scale structure and benefits on safety, stability, and therapeutic efficacy in modulating host health [56]. Consistent with these previous results, the present study revealed a key role of EVs secreted by *L. plantarum* in alleviating *C. rodentium*-induced ulcerative colitis. Further studies are needed to identify the specific molecules that are involved in the protective effects of L-EVs and investigate the underlying molecular mechanisms.

BL is a nutrient-dense plant material rich in dietary fiber, polyphenols, vitamins, and antioxidants that has been shown to favorably influence intestinal health. Its bioactive compounds contribute to maintaining gut homeostasis by modulating the composition of the gut microbiota, enhancing intestinal barrier integrity, and reducing inflammation. For example, the insoluble fibers in BL serve as substrates for beneficial bacteria, promoting the production of short-chain fatty acids (SCFAs) such as butyrate, which not only nourish colonocytes but also play a role in regulating immune responses and preserving epithelial integrity. In addition, the polyphenolic compounds act as antioxidants and anti-inflammatory agents, further supporting a balanced gut environment and potentially mitigating the risks associated with chronic inflammatory conditions.

In parallel, L-EVs represent a cutting-edge postbiotic approach to modulating gut health. These nanoscale vesicles are naturally released by the bacteria and carry a diverse array of bioactive molecules, including proteins, lipids, and nucleic acids. Through their interaction with host cells, L-EVs could modulate signaling pathways that regulate immune responses and promote tissue homeostasis. Our results suggest that they might stimulate regulatory pathways that lead to the differentiation of T regulatory cells and bolster mucosal immunity, thereby contributing to the maintenance of an optimal intestinal environment.

Together, BL and L-EVs offer a multifaceted strategy for promoting intestinal homeostasis. While BL acts as a dietary supplement that directly nourishes the gut microbiota and supports barrier function, L-EVs provide a targeted means of modulating host immune responses and reinforcing the structural and functional integrity of the gut. This dual intervention approach not only enhances the resilience of the intestinal barrier but also supports a balanced immune response, suggesting promising avenues for both preventive and therapeutic applications in gut health management. Further studies are warranted to fully elucidate the mechanisms underlying these effects and to translate these findings into clinical practice.

In conclusion, the results from our study reveal that dietary supplementation with BL ameliorates the severity of *C. rodentium*-induced enteric infection and inflammation. The beneficial effects of BL are related to the improvement of gut barrier function and suppression of pro-inflammatory Th1 immune response. Moreover, BL reduces the *C. rodentium* burden and prevents *C. rodentium*-induced gut microbiota dysbiosis by promoting the abundance of *Lactobacillus*. *L. plantarum* and its secreted EVs are identified as an important mediator required for the immunomodulatory effects of BL on pathogen infection (Fig. 11). These findings support the development of BL and L-EVs as novel intervention approaches for infection-associated colonic inflammation.

## Materials and methods

### Preparation of BL powder

The BL powder was made in accordance with our previous studies [28–30]. Briefly, fresh *Hordeum vulgare L.* leaves (cultivated in Hangzhou, China) were washed, sliced, and dried. The powdered dried barley leaves were then sifted through a 300-mesh sieve. Table S1 displays the nutritional composition of the barley leaves used in this experiment.

### Animals

Male C3H/HeN mice aged 4–6 weeks were obtained from Beijing Vital River Laboratory Animal Technology Co., Ltd. (Beijing, China) and then acclimatized under specific pathogen-free (SPF) conditions. After adaptation, mice were randomly assigned and fed a standard chow diet or an isocaloric diet, in which 2.5% BL was added. The macronutrient composition of the two diets was shown in Table S2. Animal experiments were conducted following the National Institutes of Health guide for the care and use of Laboratory Animals (NIH Publications

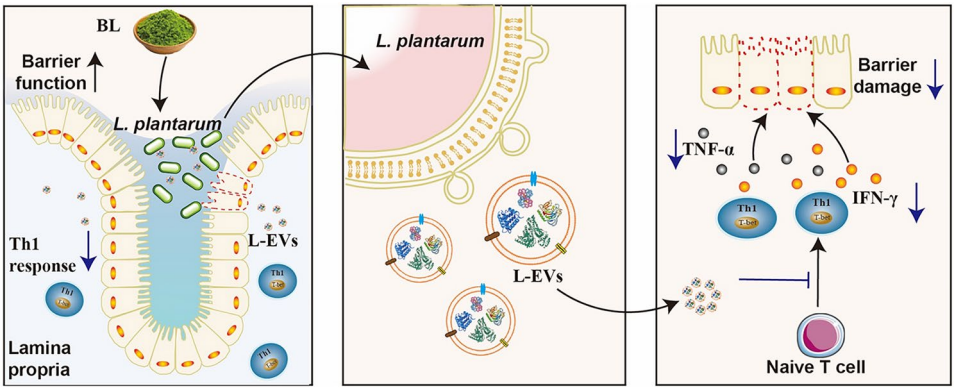


**Fig. 11** Barley leaf (BL) attenuates *C. rodentium* infection and intestinal inflammation via *L. plantarum*-derived extracellular vesicles (L-EVs). The beneficial effects of BL are related to the improvement of mucosal barrier function and suppression of pro-inflammatory T helper 1 (Th1) immune response. Moreover, BL reduces the *C. rodentium* burden and alleviates *C. rodentium*-induced gut microbiota dysbiosis by promoting the growth of *L. plantarum*. Mechanistically, EVs released by *L. plantarum* alleviate *C. rodentium*-associated pathology and T cell dysregulation. *L. plantarum* and its secreted EVs are identified as important mediators required for the immunomodulatory effects of BL on pathogen infection. This study highlights the potential use of BL, *L. plantarum* and its secreted EVs for the clinical management of infection-associated intestinal inflammatory disorders in humans

No. 8023, revised 1978), and the protocols were reviewed and approved by the Animal Care and Ethics Committee of China Agricultural University (Ethics reference number: AW32602202-4-3、AW52802202-4-1).

### C. rodentium infection

To induce bacterial colitis, mice were inoculated with approximately $1 \times 10^9$ colony forming units (CFU)/mouse of *C. rodentium* strain DBS 100 (ATCC 51459). Briefly, a single colony growing on a MacConkey agar plate (Solatbio, China) was picked and inoculated in 5 ml sterile Luria-Bertani (LB) medium overnight, then the suspension was diluted in fresh LB medium at the ratio of 1:100 and incubated at 37 ℃, centrifuged and resuspended in PBS for later mouse infestation.

### *C. rodentium* determination in mouse feces and tissues

Fresh mouse stool pellets were collected, weighed, and homogenized on days 1, 4, 7, and 10 following infection. Following that, sample homogenates were serially diluted ten-fold and plated on MacConkey agar, where *C. rodentium* colonies were counted the next day. For organ bacterial burden analysis, cecum contents, spleens and livers were collected and processed as above.

### Disease activity index (DAI)

The DAI score, which takes into account weight loss, stool consistency, and general health status, was used to assess the severity of colitis as previously described [17].

### Histological staining

The paraffin-embedded samples were sectioned, and slides were subjected to histological hematoxylin and eosin staining (H&E) before being observed with a microscope. The slides were evaluated as previously described [17].

Paraffin sections were stained with alcian blue on the manufacturer's recommendations using commercial kits (Servicebio Technology CO., Ltd., China) for goblet cell analysis. Image analysis was performed by utilizing Image J software.

### Immunofluorescence staining

After being deparaffinized and rehydrated, the paraffin-embedded sections underwent antigen retrieval using citric acid antigen retrieval buffer (pH 6.0). Slides were then 30 min later blocked in goat serum. The primary antibody used was rabbit antisera made against Ki67 (1:200; Abcam), and to specifically label the marker, CY3-conjugated goat anti-rabbit IgG (1:400; Jackson) was added as a secondary antibody. Sections were then sealed with an anti-fluorescence quenching agent after being stained with 4', 6-diamidino-2-phenylindole (DAPI; Solarbio). Under the Nikon fluorescence microscope, the pictures were observed and gathered.

### Inflammatory cytokine analysis

An enzyme-linked immunosorbent assay (ELISA) kit (Nanjing Jiancheng Bioengineering Institute Co., Ltd, China) was used to assess cytokine contents in the colon according to the manufacturer's instructions.

### Quantitative real-time PCR (RT-qPCR)

Briefly, total RNA was extracted from the colon or cecal samples stored at -80 °C utilizing the Trizol reagent (Invitrogen, USA) and reversed into cDNA according to the instructions of the FastQuant RT Kit (TianGen, China). RT-qPCR was performed using SYBR Real-time PCR Kit (Takara, Japan) by a LightCycler 480 Real-Time PCR

system (Roche, Switzerland). Data were analyzed by the $2^{-\Delta\Delta CT}$ method. The sequences of primers used in RT-qPCR are listed in Table S3.

#### 16 S rRNA gene sequencing

Total DNA extracted from mouse feces was used as a template for PCR amplification of the bacterial 16S rRNA gene's V3-V4 region. PCR amplification products from an ABI GeneAmp® 9700 PCR system (AppliedBiosystems, Foster City, CA, USA) were sequenced on the Illumina Miseq platform in Majorbio Bio-Pharm Technology Co., Ltd. (Shanghai, China) and classified into operational taxonomic units (OTUs) with a difference of 0.03 (equivalent to 97% similarity). By visualizing datasets of microbial diversity and abundance from various samples, taxonomic community structure and phylogeny were assessed. The Majorbio Cloud Platform was used for all data analysis.

#### SCFAs analysis

As previously described, the determination of SCFAs in fecal samples using gas chromatography was performed [50].

#### Fecal microbiota transplantation (FMT)

FMT was performed as previously described. Briefly, the recipient mice received a two-week treatment of combined antibiotics (neomycin, penicillin, metronidazole, 1000 mg/l; vancomycin and streptomycin 500 mg/l) before FMT to remove the native microbiota. The donor mice were fed CD or isocaloric BL chow, respectively. Fresh feces from donor mice were collected and resuspended in sterile PBS at 1:10 (m/v), vortexed, and rested, then the supernatant was taken for transplantation for three weeks. Donor and recipient mouse feces were collected for 16 S rRNA sequencing analysis upon completion of transplantation.

#### RNA-sequencing analysis

Total RNA was extracted from mouse colon tissue. The quality and RNA integrity numbers (RINs) of the extracted RNA were determined using Nanodrop2000 and Agilent2100, respectively. Then RNA sequence libraries were constructed according to the Illumina TruseqTM RNA sample prep Kit protocol. Majorbio Bio-Pharm Technology Co., Ltd. (Shanghai, China) performed sequencing of the libraries on an Illumina HiSeq2000 instrument and individually assessed for quality using FastQC. Differential expression analysis was performed by DESeq2. Genes with fold changes (FC) > 1.5 and $P$ adjust ($Padj$) < 0.05 between groups were considered as differentially expressed genes (DEGs). Statistical significance was assessed using the negative binomial Wald test, followed by correction for multiple hypothesis testing using the Benjamini-Hochberg method. Functional enrichment clustering analysis was used for the Kyoto Encyclopedia of Genes and Genomes (KEGG) pathway enrichment analysis.

#### $CD4^+$ T cell depletion

For the clearance of $CD4^+$ T cells, mice were injected intraperitoneally with anti-$CD4^+$ monoclonal antibody or its isotype control antibody once every three days at 500 μg each time for three times before and during *C. rodentium* infection.

#### Flow cytometry analysis for T cells

Single-cell suspensions were obtained by grinding mouse mesenteric lymph node and spleen tissues, incubated and stimulated with PMA, Ionomycin, Monensin, and RPMI 1640 medium (Solarbio, China), and cultured at 37 °C for 5 h under 5% $CO_2$ condition. Surface markers were stained with PerCP/Cyanine5.5 anti-mouse CD3 (Biolegend, USA), PE/Dazzle™ 594 anti-mouse CD4 antibody (Biolegend, USA), and APC anti-mouse CD25 (Biolegend, USA) for 0.5 h at 4 °C against light, then fixed and permeabilized, followed by PE/Cyanine7 anti-mouse IFN-γ (Biolegend, USA), Alexa Fluor® 488 anti-mouse IL-4 (Biolegend, USA), APC/Cyanine7 anti-mouse IL-17 A (Biolegend, USA), and PE anti-mouse FOXP3 (Biolegend, USA) intracellular staining was performed for 0.5 h. Finally, cells were detected by flow cytometry.

#### *L. plantarum* cultivation and treatment

*L. plantarum* was previously isolated by our laboratory and routinely incubated in de Man, Rogosa, and Sharpe (MRS) broth at 37 °C under anaerobic conditions. This strain was identified by morphological and physicochemical characterizations and 16 S rRNA sequence analysis. The growth of *L. plantarum* was monitored by measuring the optical density at 600 nm ($OD_{600nm}$). For *L. plantarum* treatment, *L. plantarum* was centrifuged, enriched, and resus pended in phosphate buffer solution (PBS). Mice were administered with 0.2 mL *L. plantarum* by oral gavage ($1 \times 10^9$ CFU /mL) per day for two weeks. Regarding the heat inactivation of *L. plantarum*, viability assays (plating on MRS media) were performed to verify that no residual live bacteria remained after the heat inactivation process.

#### Isolation of L-EVs

The isolation of EVs from *L. plantarum* strain culture supernatant was performed by a series of centrifugation steps as described [54, 55]. Briefly, after growing in MRS broth for 24 h, the bacterial culture solution was centrifuged at 1,000 g for 10 min. The bacteria-free culture supernatant was collected and centrifuged at 12,000 g for 30 min. Following that, the supernatant was filtered

via a 0.22 μm bottle top filter (Corning, NY) to remove any cell debris from the medium. The L-EVs pellets were obtained by ultracentrifugation at 12,000 g for 3 h at 4 °C. Finally, purified L-EVs were suspended in PBS and stored at -80 ℃ until further use. For L-EVs treatment, mice were orally administered 50 μg of L-EVs per day for two weeks.

### Characterization of L-EVs

Morphological characteristics of *L. plantarum* and L-EVs were detected by scanning electron microscopy (SEM). Samples were fixed with 2.5% PBS-diluted glutar aldehyde. After being rinsed three times in PBS, samples were post-fixed in 1% osmium tetroxide for 1 h, dehydrated in alcohol, and then critical-point-dried using $CO_2$. The samples were coated with gold and observed in a Hitachi S-3400 scanning electron microscope (Hita chi, Japan).

The morphology of the L-EVs was observed using transmission electron microscope (TEM). For sample preparation, L-EVs were fixed with 2.5% glutaraldehyde and were then fixed with 1% osmium tetroxide at 4 °C for 2 h, dehydrated in acetone. Next, the samples were post-fixed in 2% osmium tetroxide for 1 h and 1% uranylacetate. The sections were post-stained with uranyl acetate and lead citrate then examined under a H-7650 transmission electron microscope (Hitachi, Japan).

### Nanoparticle tracking analysis

The particle size and number of L-EVs was quantified using the ZetaView PMX 110 particle analyzer under 405 nm excitation light. Laser light was used to irradiate the nanoparticle suspension, and the scattered light from the nanoparticles was detected. The nanoparticle concentration was calculated by counting the scattered particles.

### Proteomic analysis

Briefly, L-EVs were lysed on ice by sonication in buffer containing 8 M urea, 1% protease inhibitor cocktail and 2 mM EDTA. Following centrifugation at 12 000×g for 15 min at 4℃, protein concentrations of the supernatants were determined by BCA assay. Extracted proteins (100 μg per replicate) were reduced, alkylated and then digested with sequencing-grade trypsin (Promega, #V5111) at a 1:50 (w/w) enzyme: protein ratio overnight at 37℃. The resulting peptide mixtures were fractionated by high-pH reversed-phase HPLC and each fraction analyzed by UPLC-MS/MS on a Q Exactive™ Plus mass spectrometer (Thermo Fisher Scientific) coupled online to an Easy-nLC 1200 system. Data-independent acquisition was employed. Raw spectra were searched against the draft genome of *L. plantarum* in the UniProt database using MaxQuant (v1.6). The biological function of the identified proteins was classified by Gene Ontology (GO) annotation from the UniProt-GOA database. KEGG pathway database was used to analyze the metabolic pathways involved in the differentially expressed proteins.

### Distribution of L-EVs in vivo

L-EVs were incubated with the fluorescent dye DiR at 37 ℃for 1 h, after which DiR-labeled L-EVs were isolated by ultracentrifugation and resuspended in PBS. Each mouse was gavaged with DiR-labeled L-EVs at 500 μg/200μL PBS. The distribution of L-EVs was visualized by in vivo imaging using an Odyssey CLx imaging system (LI-COR Biosciences, Lincoln, NE, USA) at 8 h after administration.

### Biosafety evaluation of L-EVs in vivo

Six-week-old C57BL/6 mice were randomly divided into four groups: Control, L-L-EVs (25 μg/d), M-L-EVs (50 μg/d) and H-L-EVs (100 μg/d). These L-EVs were administered daily for a total of 12 times. The changes in the body weight and food intake of the mice were recorded. Then, blood from the mice was collected, and the concentrations of TNF-α and IFN-γ in the serum were measured. The major organs (liver, spleen and colon) were subsequently collected for further H&E staining.

### Statistics

Statistical analysis was carried out using Prism 6.0 (GraphPad Software, CA). Data are presented as means ± SEM. Significant differences between the two groups were evaluated by a two-tailed unpaired Student's *t*-test. Significant differences in more than two groups were evaluated by one-way or two-way analysis of variance (ANOVA) followed by Tukey's multiple comparisons test.

## Supplementary Information

The online version contains supplementary material available at https://doi.org/10.1186/s12951-025-03504-w.

Supplementary Material 1

#### Acknowledgements

The authors would like to thank Dr. Fang Zhou (College of Health Solutions, Arizona State University) for critical reading of this manuscript.

#### Author contributions

Y.F. conceived the research idea, designed the experimental plan, conducted the experiments, collected and organized data, drafted the initial manuscript, and conducted data analysis.Q.Z. and Y.Z. organized data, and participated in manuscript revision.C.M., M. T., X. H. and F.C. provided technical support and optimized experimental methods.D.L. supervised the research process, provided funding support, and contributed to manuscript review and finalization.

**Funding**
This work was supported by the National Natural Science Foundation of China (grant number 32371511 and 32001677) and the China Postdoctoral Science Foundation (grant number 2020M680256).

**Data availability**
No datasets were generated or analysed during the current study.

## Declarations

**Ethics approval**
The animal protocols were reviewed and approved by the Animal Care and Ethics Committee of China Agricultural University (Ethics reference number: AW32602202-4-3 and AW52802202-4-1).

**Competing interests**
The authors declare no competing interests.

**Author details**
[1]Center for Fruit and Vegetable Processing, Key Laboratory of Fruits and Vegetables Processing, Engineering Research Centre for Fruits and Vegetable Processing, Ministry of Agriculture, Ministry of Education, China Agricultural University, Beijing 100083, China
[2]College of Food Science and Nutritional Engineering, China Agricultural University, No. 17, Qinghua East Road, Haidian District, Beijing 100083, China

Received: 26 February 2025 / Accepted: 27 May 2025
Published online: 07 June 2025

**References**

1. Torres J, Mehandru S, Colombel JF, Peyrin-Biroulet L. Crohn's disease. Lancet. 2017;389:1741–55.
2. Ungaro R, Mehandru S, Allen PB, Peyrin-Biroulet L, Colombel JF. Ulcerative colitis. Lancet. 2017;389:1756–70.
3. Ng SC, Tang W, Ching JY, Wong M, Chow CM, Hui AJ, Wong TC, Leung VK, Tsang SW, Yu HH, et al. Incidence and phenotype of inflammatory bowel disease based on results from the Asia-Pacific crohn's and colitis epidemiology study. Gastroenterology. 2013;145:158–65.
4. Kaplan GG, Ng SC. Understanding and preventing the global increase of inflammatory bowel disease. Gastroenterology. 2017;152:313–21.
5. Ng SC, Shi HY, Hamidi N, Underwood FE, Tang W, Benchimol EI, Panaccione R, Ghosh S, Wu JCY, Chan FKL, et al. Worldwide incidence and prevalence of inflammatory bowel disease in the 21st century: a systematic review of population-based studies. Lancet. 2017;390:2769–78.
6. Danese S. New therapies for inflammatory bowel disease: from the bench to the bedside. Gut. 2012;61:918–32.
7. Pickard JM, Zeng MY, Caruso R, Núñez G. Gut microbiota: role in pathogen colonization, immune responses, and inflammatory disease. Immunol Rev. 2017;279:70–89.
8. Sommer F, Anderson JM, Bharti R, Raes J, Rosenstiel P. The resilience of the intestinal microbiota influences health and disease. Nat Rev Microbiol. 2017;15:630–8.
9. Xavier RJ, Podolsky DK. Unravelling the pathogenesis of inflammatory bowel disease. Nature. 2007;448:427–34.
10. Bolte LA, Vich Vila A, Imhann F, Collij V, Gacesa R, Peters V, Wijmenga C, Kurilshikov A, Campmans-Kuijpers MJE, Fu J, et al. Long-term dietary patterns are associated with pro-inflammatory and anti-inflammatory features of the gut Microbiome. Gut. 2021;70:1287–98.
11. Hou JK, Abraham B, El-Serag H. Dietary intake and risk of developing inflammatory bowel disease: A systematic review of the literature. Am J Gastroenterol. 2011;106:563–73.
12. Fritsch J, Garces L, Quintero MA, Pignac-Kobinger J, Santander AM, Fernández I, Ban YJ, Kwon D, Phillips MC, Knight K, et al. Low-Fat, High-Fiber diet reduces markers of inflammation and dysbiosis and improves quality of life in patients with ulcerative colitis. Clin Gastroenterol Hepatol. 2021;19:1189–99.
13. Levine A, Sigall Boneh R, Wine E. Evolving role of diet in the pathogenesis and treatment of inflammatory bowel diseases. Gut. 2018;67:1726–38.
14. Luperchio SA, Schauer DB. Molecular pathogenesis of Citrobacter rodentium and transmissible murine colonic hyperplasia. Microbes Infect. 2001;3:333–40.
15. Kamada N, Sakamoto K, Seo SU, Zeng MY, Kim YG, Cascalho M, Vallance BA, Puente JL, Núñez G. Humoral immunity in the gut selectively targets phenotypically virulent attaching-and-effacing bacteria for intraluminal elimination. Cell Host Microbe. 2015;17:617–27.
16. Mullineaux-Sanders C, Sanchez-Garrido J, Hopkins EGD, Shenoy AR, Barry R, Frankel G. Citrobacter rodentium–host–microbiota interactions: immunity, bioenergetics and metabolism. Nat Rev Microbiol. 2019;17:701–15.
17. Collins JW, Keeney KM, Crepin VF, Rathinam VAK, Fitzgerald KA, Finlay BB, Frankel G. Citrobacter rodentium: infection, inflammation and the microbiota. Nat Rev Microbiol. 2014;12:612–23.
18. Thaiss CA, Levy M, Grosheva I, Zheng D, Soffer E, Blacher E, Braverman S, Tengeler AC, Barak O, Elazar M, et al. Hyperglycemia drives intestinal barrier dysfunction and risk for enteric infection. Science. 2018;359:1376–83.
19. Vallance BA, Deng W, Knodler LA, Finlay BB. Mice lacking T and B lymphocytes develop transient colitis and crypt hyperplasia yet suffer impaired bacterial clearance during Citrobacter rodentium infection. Infect Immun. 2002;70:2070–81.
20. Shiomi H, Masuda A, Nishiumi S, Nishida M, Takagawa T, Shiomi Y, Kutsumi H, Blumberg RS, Azuma T, Yoshida M. Gamma interferon produced by antigen-specific CD4 + T cells regulates the mucosal immune responses to Citrobacter rodentium infection. Infect Immun. 2010;78:2653–66.
21. Hoffmann C, Hill DA, Minkah N, Kirn T, Troy A, Artis D, Bushman F. Community-wide response of the gut microbiota to enteropathogenic Citrobacter rodentium infection revealed by deep sequencing. Infect Immun. 2009;77:4668–78.
22. Wiles S, Clare S, Harker J, Huett A, Young D, Dougan G, Frankel G. Organ specificity, colonization and clearance dynamics in vivo following oral challenges with the murine pathogen Citrobacter rodentium. Cell Microbiol. 2004;6:963–72.
23. Kamada N, Kim YG, Sham HP, Vallance BA, Puente JL, Martens EC, Núñez G. Regulated virulence controls the ability of a pathogen to compete with the gut microbiota. Science. 2012;336:1325–9.
24. Neumann M, Steimle A, Grant ET, Wolter M, Parrish A, Willieme S, Brenner D, Martens EC, Desai MS. Deprivation of dietary fiber in specific-pathogen-free mice promotes susceptibility to the intestinal mucosal pathogen Citrobacter rodentium. Gut Microbes. 2021;13(1):1966263.
25. Ferreres F, Kršková Z, Gonçalves RF, Valentão P, Pereira JA, Dušek J, Martin J, Andrade PB. Free water-soluble phenolics profiling in barley (Hordeum vulgare L). J Agric Food Chem. 2009;57:2405–9.
26. Yu YM, Chang WC, Chang CT, Hsieh CL, Tsai CE. Effects of young barley leaf extract and antioxidative vitamins on LDL oxidation and free radical scavenging activities in type 2 diabetes. Diabetes Metab. 2002;28:107–14.
27. Yamaura K, Nakayama N, Shimada M, Bi Y, Fukata H, Ueno K. Antidepressant-like effects of young green barley leaf (Hordeum vulgare L.) in the mouse forced swimming test. Pharmacognosy Res. 2012;4:22–6.
28. Tian M, Li D, Ma C, Feng Y, Hu X, Chen F. Barley leaf insoluble dietary fiber alleviated dextran sulfate sodium-induced mice colitis by modulating gut microbiota. Nutrients. 2021;13:1–19.
29. Li D, Feng Y, Tian M, Ji J, Hu X, Chen F. Gut microbiota-derived inosine from dietary barley leaf supplementation attenuates colitis through PPARγ signaling activation. Microbiome. 2021;9.
30. Li D, Feng Y, Tian M, Hu X, Zheng R, Chen F. Dietary barley leaf mitigates tumorigenesis in experimental colitis-associated colorectal cancer. Nutrients. 2021;13.
31. Dicks LMT. How important are fatty acids in human health and can they be used in treating diseases? Gut Microbes. 2024;16(1):2420765.
32. Koh A, De Vadder F, Kovatcheva-Datchary P, Bäckhed F. From dietary fiber to host physiology: Short-chain fatty acids as key bacterial metabolites. Cell. 2016;165:1332–45.
33. Sun M, Wu W, Chen L, Yang W, Huang X, Ma C, Chen F, Xiao Y, Zhao Y, Ma C et al. Microbiota-derived short-chain fatty acids promote Th1 cell IL-10 production to maintain intestinal homeostasis. Nat Commun. 2018;9.
34. Chen L, Sun M, Wu W, Yang W, Huang X, Xiao Y, Ma C, Xu L, Yao S, Liu Z, et al. Microbiota metabolite butyrate differentially regulates Th1 and Th17 cells' differentiation and function in induction of colitis. Inflamm Bowel Dis. 2019;25:1450–61.
35. Hao H, Zhang X, Tong L, Liu Q, Liang X, Bu Y, Gong P, Liu T, Zhang L, Xia Y, Ai L, Yi H. Effect of extracellular vesicles derived from Lactobacillus plantarum

Q7 on gut microbiota and ulcerative colitis in mice. Front Immunol. 2021;12:777147.
36. Li YJ, Zhang C, Martincuks A, et al. STAT proteins in cancer: orchestration of metabolism. Nat Rev Cancer. 2023;23(3):115–34.
37. Zhang C, Chen S, Wang Z, et al. Exploring the mechanism of intestinal bacterial translocation after severe acute pancreatitis: the role of Toll-like receptor 5. Gut Microbes. 2025;17(1):2489768.
38. Yin S, Peng Y, Lin YR, et al. Bacterial heat shock protein: a new crosstalk between T lymphocyte and macrophage via JAK2/STAT1 pathway in bloodstream infection. Microbiol Res. 2024;282:127626.
39. Geng C, He S, Yu S, et al. Achieving clearance of Drug-Resistant bacterial infection and rapid cutaneous wound regeneration using an ROS-Balancing-Engineered heterojunction. Adv Mater. 2024;36(16):2310599.
40. Yu YM, Chang WC, Liu CS, Tsai CM. Effect of young barley leaf extract and adlay on plasma lipids and LDL oxidation in hyperlipidemic smokers. Biol Pharm Bull. 2004;27:802–5.
41. Lopez CA, Miller BM, Rivera-Chávez F, Velazquez EM, Byndloss MX, Chávez-Arroyo A, Lokken KL, Tsolis RM, Winter SE, Bäumler AJ. Virulence factors enhance Citrobacter rodentium expansion through aerobic respiration. Science. 2016;353:1249–53.
42. Peterson LW, Artis D. Intestinal epithelial cells: regulators of barrier function and immune homeostasis. Nat Rev Immunol. 2014;14:141–53.
43. Desai MS, Seekatz AM, Koropatkin NM, Kamada N, Hickey CA, Wolter M, Pudlo NA, Kitamoto S, Terrapon N, Muller A, et al. A dietary Fiber-Deprived gut microbiota degrades the colonic mucus barrier and enhances pathogen susceptibility. Cell. 2016;167:1339–53.
44. Kumar A, Priyamvada S, Ge Y, Jayawardena D, Singhal M, Anbazhagan AN, Chatterjee I, Dayal A, Patel M, Zadeh K, et al. A novel role of SLC26A3 in the maintenance of intestinal epithelial barrier integrity. Gastroenterology. 2021;160:1240–55.
45. Stockinger B. T cell subsets and environmental factors in Citrobacter rodentium infection. Curr Opin Microbiol. 2021;63:92–7.
46. Higgins LM, Frankel G, Douce G, Dougan G, MacDonald TT. Citrobacter rodentium infection in mice elicits a mucosal Th1 cytokine response and lesions similar to those in murine inflammatory bowel disease. Infect Immun. 1999;67:3031–9.
47. Ott SJ, Musfeldt M, Wenderoth DF, Hampe J, Brant O, Fölsch UR, Timmis KN, Schreiber S. Reduction in diversity of the colonic mucosa associated bacterial microflora in patients with active inflammatory bowel disease. Gut. 2004;53:685–93.
48. Manichanh C, Rigottier-Gois L, Bonnaud E, Gloux K, Pelletier E, Frangeul L, Nalin R, Jarrin C, Chardon P, Marteau P, et al. Reduced diversity of faecal microbiota in crohn's disease revealed by a metagenomic approach. Gut. 2006;55:205–11.
49. Shin NR, Whon TW, Bae JW. Proteobacteria: microbial signature of dysbiosis in gut microbiota. Trends Biotechnol. 2015;33:496–503.
50. Li D, Wang P, Wang P, Hu X, Chen F. Gut microbiota promotes production of aromatic metabolites through degradation of barley leaf fiber. J Nutr Biochem. 2018;58:49–58.
51. Wu H, Xie S, Miao J, Li Y, Wang Z, Wang M, Yu Q. Lactobacillus reuteri maintains intestinal epithelial regeneration and repairs damaged intestinal mucosa. Gut Microbes. 2020;11:997–1014.
52. Zhang Y, Mu T, Yang Y, Zhang J, Ren F, Wu Z. Lactobacillus johnsonii attenuates Citrobacter rodentium-Induced colitis by regulating inflammatory responses and Endoplasmic reticulum stress in mice. J Nutr. 2021;151:3391–9.
53. van Niel G, D'Angelo G, Raposo G. Shedding light on the cell biology of extracellular vesicles. Nat Rev Mol Cell Biol. 2018;19(4):213–28.
54. Tao S, Fan J, Li J, Wu Z, Yao Y, Wang Z, Wu Y, Liu X, Xiao Y, Wei H. Extracellular vesicles derived from Lactobacillus johnsonii promote gut barrier homeostasis by enhancing M2 macrophage polarization. J Adv Res. 2024:S2090-1232(24)00111-5.
55. Hu R, Lin H, Wang M, Zhao Y, Liu H, Min Y, Yang X, Gao Y, Yang M. Lactobacillus reuteri-derived extracellular vesicles maintain intestinal immune homeostasis against lipopolysaccharide-induced inflammatory responses in broilers. J Anim Sci Biotechnol. 2021;12(1):25.
56. Chen X, Li Q, Xie J, Nie S. Immunomodulatory effects of Probiotic-Derived extracellular vesicles: opportunities and challenges. J Agric Food Chem. 2024;72(35):19259–73.

## Publisher's note